

This is a repository copy of *Trace and major element incorporation into amorphous calcium carbonate (ACC) precipitated from seawater*.

White Rose Research Online URL for this paper:

<https://eprints.whiterose.ac.uk/165260/>

Version: Accepted Version

Article:

Evans, David, Gray, William R., Rae, James W.B. et al. (5 more authors) (2020) Trace and major element incorporation into amorphous calcium carbonate (ACC) precipitated from seawater. *Geochimica et Cosmochimica Acta*. pp. 293-311. ISSN 0016-7037

<https://doi.org/10.1016/j.gca.2020.08.034>

Reuse

Items deposited in White Rose Research Online are protected by copyright, with all rights reserved unless indicated otherwise. They may be downloaded and/or printed for private study, or other acts as permitted by national copyright laws. The publisher or other rights holders may allow further reproduction and re-use of the full text version. This is indicated by the licence information on the White Rose Research Online record for the item.

Takedown

If you consider content in White Rose Research Online to be in breach of UK law, please notify us by emailing eprints@whiterose.ac.uk including the URL of the record and the reason for the withdrawal request.

1 **Trace and major element incorporation into amorphous calcium carbonate**

2 **(ACC) precipitated from seawater**

3 David Evans^{1*†}, William R. Gray^{1,2}, James W. B. Rae¹, Rosanna Greenop¹, Paul B. Webb³, Kirsty
4 Penkman⁴, Roland Kröger⁵, & Nicola Allison¹

5 ¹ School of Earth and Environmental Sciences, University of St Andrews, St Andrews, UK

6 ² Laboratoire des Sciences du Climat et de l'Environnement (LSCE/IPSL), Gif-sur-Yvette, France

7 ³ School of Chemistry, University of St Andrews, St Andrews, UK

8 ⁴ BioArCh, Department of Chemistry, University of York, York, UK

9 ⁵ Department of Physics, University of York, York, UK

10 * Now at: Institute for Geosciences, Goethe University Frankfurt, 60438 Frankfurt am Main, Germany

11 † evans@em.uni-frankfurt.de

12

13 **Abstract**

14 Amorphous calcium carbonate (ACC) has been identified or inferred to exist in many groups of
15 marine organisms that produce biominerals widely used as geochemical archives (e.g. foraminifera,
16 molluscs, echinoderms). However, little is known about trace element incorporation into ACC, and
17 thus it is not understood how precipitation through an ACC precursor might impact the fidelity of
18 climate proxies and biomineralisation models built on the skeletal geochemistry of these marine
19 calcifiers. To address this, we investigated the incorporation of Li, B, Na, Mg, Mn, Sr, Ba, and U into
20 inorganic amorphous calcium magnesium carbonates precipitated from seawater under a variety of
21 different carbonate chemistries, Mg/Ca ratios, and in the presence of aspartic and glutamic acid, two
22 of the most common intracrystalline amino acids found in foraminifera and corals. ACC is highly
23 enriched in most of these trace elements relative to the crystalline carbonates yet similar in some
24 respects in terms of the factors influencing trace element partitioning. For example, ACC B/Ca is
25 sensitive to the carbonate system, whilst Mg/Ca and Sr/Ca are largely a function of their respective
26 ratio in seawater. In general, we find that most of the variance in the distribution coefficients of the
27 other trace elements can be explained by some combination of the seawater carbonate chemistry and
28 the seawater or ACC Mg/Ca ratio.

29 **1. Introduction**

30 Geochemical proxies based on the (trace) elemental or isotopic composition of carbonate minerals are
31 important tools for understanding past environmental changes. While such proxies are typically
32 empirically calibrated, understanding the mechanistic basis of these techniques is key to identifying
33 instances in which further calibration is necessary, or when existing calibrations may not be
34 applicable. As such, knowledge of the geochemistry of ACC is required to understand how
35 precipitation through an amorphous precursor might impact our understanding or interpretation of
36 CaCO₃-hosted proxy systems, which form the basis of a substantial portion of our knowledge of
37 palaeoceanography and palaeoclimatology.

38

39 In addition, much of our understanding of the biomineralisation process of calcifying marine
40 organisms is derived from the comparison of skeletal chemical data to inorganically precipitated
41 carbonates (Bentov and Erez, 2006; Gagnon et al., 2012; de Nooijer et al., 2014; Decarlo et al., 2018).
42 These forward modelling exercises are based on elemental partition coefficients and isotopic
43 fractionation factors into calcite and aragonite, which may enable the conditions at the calcification
44 site to be reconstructed. For example, the inorganic calcite Mg distribution coefficient (D_{Mg}) is 1-2
45 orders of magnitude higher than the apparent D_{Mg} of planktonic foraminifera (Mucci and Morse,
46 1983; Bentov and Erez, 2006; De Choudens-Sanchez and Gonzalez, 2009). The most parsimonious
47 explanation for this difference is that these organisms likely reduce the Mg/Ca ratio of their calcifying
48 environment in order to produce low-Mg calcite (Erez, 2003; Evans et al., 2018), highlighting how a
49 relatively simple comparison can form the basis of an important component of a calcification model.
50 One of the fundamental assumptions made by this approach is that CaCO₃ precipitation by marine
51 organisms is analogous to inorganic precipitation from a (semi)enclosed environment that is modified
52 in its elemental and/or carbonate chemistry with respect to seawater. However, it has since been
53 found, or inferred, that several major groups of marine calcifiers precipitate through an amorphous
54 precursor phase (Beniash et al., 1997; Politi et al., 2006; Sviben et al., 2016; Jacob et al., 2017). This
55 potentially poses a complication for the inference of calcification site conditions from skeletal
56 geochemistry because little is known about the distribution coefficients of trace elements in
57 amorphous calcium carbonate (ACC), so an important step is missing from current models. This is of
58 particular concern because previous studies have shown that the chemistry of ACC differs greatly
59 from crystalline CaCO₃. For example, ACC D_{Mg} is >2 times higher than calcite (Blue and Dove, 2015).

60 Knowledge of the ACC precursor phase is important because the transformation of ACC to crystalline
61 CaCO_3 must take place in the (semi)closed environment of the calcification space. Depending on the
62 ACC/seawater ratio at the calcification site, the composition of ACC has the potential to greatly
63 impact the solution elemental chemistry during the transformation process, even if the ACC-calcite
64 transformation can take place through a dissolution-reprecipitation reaction (Giuffrè et al., 2015).

65

66 Assessing the sensitivity of proxy systems and biomineralisation models to precipitation through an
67 ACC precursor is challenging because few studies of trace element incorporation into ACC exist.
68 Furthermore, the geochemistry of ACC precipitated under conditions relevant to marine organisms
69 has so far not been studied, i.e. from seawater rather than ionically simpler solutions. In order to
70 address this, we present trace and major element data of amorphous carbonates precipitated from
71 seawater-based solutions under a wide range of conditions, varying pH and DIC, the trace element/Ca
72 ratio of seawater, the seawater $[\text{Mg}^{2+}]$, and the concentration of two amino acids relevant to
73 biomineralisation (aspartic and glutamic acid; Asp, Glu). Because seawater has a Mg/Ca ratio of 5.2,
74 the samples discussed here are likely amorphous calcium magnesium carbonates rather than pure
75 ACC. However, we use the term ACC throughout as amorphous carbonates precipitated from
76 seawater have a Mg/Ca ratio <1 , and there is no formal definition of the difference between these
77 terms.

78

79 **2. Materials & Methods**

80 Four principal experiments were conducted: 1) A pH experiment, in which pH (8.95-10.36) and DIC
81 (2.8-22.8 mM) broadly covaried as we were unable to produce ACC from (e.g.) low-pH, low-DIC
82 seawater, 2) A seawater $[\text{Mg}^{2+}]$ experiment, in which the Mg concentration was varied between ~0-50
83 mM at constant $[\text{Ca}^{2+}]$, 3) A seawater $[\text{Ca}^{2+}]$ experiment, in which the Ca concentration was varied
84 between ~20-50 mM at constant $[\text{Mg}^{2+}]$, and 4) An amino acid experiment, in which Asp and/or Glu
85 were added up to a total concentration of 40 mM. This upper amino acid concentration is far in excess
86 of that likely to be present at the calcification site of marine organisms (e.g. compare King and Hare
87 (1972) and Kim et al. (2016)), which is extended here in order to better mechanistically understand
88 the effect of the presence of these molecules. The precipitation dynamics of some of these experiments
89 were previously described in Evans et al. (2019).

90

91 **2.1 ACC precipitation and seawater carbonate chemistry**

92 All experiments were conducted in artificial seawater ($I = 0.72$) made according to the recipe of
93 Millero (2013) with the addition of several trace elements of interest at approximate open ocean
94 concentrations (Li, Mn, Zn, Sr, Ba, the REE, and U), see the supplementary material. In some
95 experiments the seawater Mg/Ca ratio was manipulated either by spiking 'normal' artificial seawater
96 (Mg/Ca = 53/10.3 mM) with CaCl_2 , or by spiking Mg-free artificial seawater with MgCl_2 (otherwise
97 produced using the same recipe). Salinity was not adjusted in these experiments, such that it scaled
98 with increasing $[\text{Ca}^{2+}]$ up to 37 PSU (50 mM Ca^{2+} ; $I = 0.84$) and decreasing $[\text{Mg}^{2+}]$ down to 33 PSU
99 (Mg-free seawater; $I = 0.56$). In the case of experiments conducted in the presence of amino acids, the
100 desired amount of salt was weighed and added to the seawater immediately before the start of
101 individual experiments. After the addition of the amino acid the solution was stirred vigorously for
102 10-15 minutes to ensure full dissolution, following which the carbonate system was readjusted to the
103 desired conditions.

104
105 ACC was precipitated from seawater using a Metrohm 902 Titrand titrator as described in detail in
106 Evans et al. (2019). In all cases precipitation took place in 250 ml of seawater placed into an acid-
107 cleaned HDPE beaker (1 M HCl). Before every experiment the titrant dosing tubes and electrodes
108 were cleaned in weak (0.1 M) HCl to ensure no residual precipitate from the previous titration. Prior
109 to beginning the experiment, the seawater carbonate chemistry was adjusted close to the desired value
110 by slowly pipetting 1 M Na_2CO_3 during rapid stirring, following which the pH was modified through
111 NaOH or HCl addition, monitored using a calibrated pH electrode (using traceable NBS buffers). A
112 calibrated Ca electrode (using seawaters with measured $[\text{Ca}^{2+}]$) was monitored throughout this time to
113 ensure that no precipitation took place while the carbonate chemistry was being adjusted. Once the
114 desired pH and DIC values were reached, ACC precipitation was induced by controlled simultaneous
115 titration of 0.45 M CaCl_2 and Na_2CO_3 solutions, added in most cases at a rate of 0.5 ml min^{-1} (see Tab.
116 1), whilst slowly stirring the solution throughout the precipitation process. Seawater temperature was
117 approximately equivalent to room temperature, varying by $<1.2^\circ\text{C}$ within a titration, with a
118 $\text{mean} \pm 2\text{SD}$ of $22.5 \pm 2.1^\circ\text{C}$ across all experiments. The seawater and precipitate were immediately
119 separated at the end of the experiment by vacuum filtration using a $0.2 \mu\text{m}$ nylon membrane filter.
120 The precipitate was thoroughly washed four times with trace element-grade ethanol, air-dried, and
121 stored in acid-cleaned micro centrifuge tubes. Sub samples of the filtered seawater were taken for DIC

122 analysis (performed immediately, see Sec. 2.3) and elemental chemistry. The latter were acidified to
123 5% HNO₃ for storage in an acid-cleaned polypropylene centrifuge tube. All plastic used to store
124 samples was pre-cleaned with 1 M HCl.

125

126 The experimental setup is designed such that precipitation did not take place immediately, but after a
127 relatively small degree of titration. In order to relate the precipitate geochemistry to the precise
128 solution chemistry conditions at the onset of ACC precipitation, rather than the seawater reservoir,
129 the pH and [Ca²⁺] electrodes were used to monitor the evolution of the seawater chemistry through
130 the titration. The DIC and [Ca²⁺] at the onset of precipitation were calculated based on the deviation
131 of the electrode-derived [Ca²⁺] titration curve from that predicted if all titrated CaCl₂ remained in
132 solution (see Evans et al. (2019) for a detailed explanation). For example, [Ca²⁺] at the onset of
133 precipitation equals the initial seawater [Ca²⁺] plus the total titrated CaCl₂ at the point at which the
134 titration curve diverged from predicted. The seawater trace element/Ca ratio at the onset of
135 precipitation was calculated using the trace element concentrations of the seawater reservoir and the
136 [Ca²⁺] at the onset of precipitation, and it was this ratio that was used to calculate trace element
137 distribution coefficients. For example, $Mg/Ca_{sw} = [Mg^{2+}]_{initial}/([Ca^{2+}]_{initial} + [Ca^{2+}]_{titrated})$, such that $D_{Mg} =$
138 $(Mg/Ca_{precipitate})/([Mg^{2+}]_{initial}/([Ca^{2+}]_{initial} + [Ca^{2+}]_{titrated}))$. Precipitation typically preceded for <7 minutes
139 (Tab. S4), during which time the electrodes were monitored until the precipitate and seawater were
140 separated. In the case of experiments that yielded ACC, the mean 4RSD variation in [Ca²⁺] between
141 the initiation of precipitation and the end of the experiment was 1.6% (maximum within any given
142 experiment 5%), which we do not consider a significant source of uncertainty in the calculation of the
143 distribution coefficients reported here. For experiments resulting in ACC precipitation, seawater pH
144 variation between the onset of precipitation and the end of the experiment was <0.03 units.
145 Experiments dominantly yielding calcite were characterised by a wider variation in pH (typically <0.1
146 units) and [Ca²⁺]; the data are presented for comparison but are not discussed or interpreted here.

147

148 The seawater saturation state at the onset of precipitation was derived from the calculated [Ca²⁺] and
149 DIC values, and the measured pH at the relevant point in the titration, using co2sys (Lewis and
150 Wallace, 1998) with the constants of Dickson and Millero (1987) and Dickson (1990). While several
151 studies have investigated ACC and amorphous calcium magnesium carbonate (ACMC) solubility (e.g.
152 Brecevic and Nielsen, 1989; Purgstaller et al., 2019), this work has demonstrated that the solubility of

153 ACCM is strongly dependent on the Mg concentration of the solid phase and other factors. Because
154 experimental solubility data are not reported here, and given that it is not known how the
155 composition of ACC precipitated from seawater might differ from previous studies in a way that
156 might affect solubility, we report saturation state simply as the $[\text{Ca}^{2+}][\text{CO}_3^{2-}]$ product.

157

158 **2.2 Precipitate characterisation**

159 The type of material precipitated was assessed through Raman spectroscopy and attenuated total
160 reflectance Fourier-transform infrared spectroscopy (ATR-FTIR), as ACC can be readily
161 distinguished from the crystalline polymorphs of CaCO_3 using these techniques (e.g. Andersen and
162 Brečević, 1991). Raman measurements were collected using a Horiba Jobin Yvon LabRam HR800 with
163 a 50× long-working-distance objective lens, an excitation wavelength of 514 nm, beam diameter of 1
164 μm , and a spectral resolution of $\sim 1.8 \text{ cm}^{-1}$. Samples were initially analysed with a low laser energy
165 (1%), which was gradually increased to maximise signal/noise whilst ensuring no laser-induced
166 alteration of the amorphous samples took place. All scans were performed 20×5 times, and no
167 processing was applied except for a linear fluorescent baseline subtraction. ATR-FTIR spectra were
168 collected using a Bruker Platinum ATR infrared spectrometer fitted with a TGS detector (see the
169 supplementary material). A baseline measurement was performed before the analysis of every sample,
170 measurements were performed at 1.4 cm^{-1} resolution with 32 scans. TGA-MS curves of some of the
171 precipitates discussed here have been previously reported (see Evans et al., 2019).

172

173 Precipitates were analysed for their major/trace element/Ca ratios using an Agilent 7500a inductively
174 coupled plasma mass spectrometer (ICPMS) in the StAiG laboratory, University of St Andrews.
175 Because of the possibility of ACC spontaneously transforming into a crystalline carbonate in the
176 centrifuge tubes in which the samples were stored (Konrad et al., 2016), the entire sample was first
177 dissolved in weak ($\sim 0.1 \text{ M}$) HNO_3 without transfer to avoid possible preferential selection of
178 crystalline CaCO_3 or ACC. Once fully dissolved, all samples were centrifuged to remove any shards of
179 the membrane filter and the supernatant transferred to a clean centrifuge tube. Next, an aliquot from
180 each of these centrifuged samples was diluted 30:1 in 0.5 M HNO_3 and analysed for its $[\text{Mg}^{2+} + \text{Ca}^{2+}]$.
181 Once determined, a second aliquot of each sample was diluted to $1 \text{ mM } [\text{Mg}^{2+} + \text{Ca}^{2+}]$ and reanalysed
182 for the following masses (m/z): ^7Li , ^{11}B , ^{23}Na , ^{25}Mg , ^{43}Ca , ^{48}Ca , ^{55}Mn , ^{88}Sr , ^{138}Ba , and ^{238}U . Blank and
183 standard measurements were performed every fifth sample. Raw counts were converted into

184 element/Ca ratios via blank subtraction, ratioing to ^{43}Ca , and standardisation using a multi-element
185 solution with the same $[\text{Ca}^{2+}]$ of the samples and a trace element composition similar to low-Mg
186 foraminiferal calcite. Accuracy and precision were assessed by repeat analysis of three in-house multi-
187 element standards with trace element concentrations comparable to the samples. The only exception
188 to this was Mg/Ca, which is 1-2 orders of magnitude higher in ACC compared to the crystalline
189 CaCO_3 routinely analysed using this protocol. In order to confirm the linearity of the response of the
190 mass spectrometer at the high Mg/Ca ratios of the ACC samples, one of the in-house standards was
191 spiked with a single element ICPMS Mg standard to a calculated Mg/Ca ratio of 353 mmol/mol.
192 Repeat measurement of this modified standard yielded a value 6% higher, which likely results from
193 the extrapolation of the uncertainty in the primary standard to these relatively high Mg/Ca ratios.
194 Nonetheless, the precision of repeat measurements of the high Mg/Ca standard was <1% such that we
195 can precisely resolve relative differences between samples, although an uncertainty of 6% should be
196 applied to our Mg/Ca data when comparing to other studies.

197

198 Based on 26 analyses of three in-house standards analysed over the same time interval as the samples
199 (except in the case of Mg, see above), analytical precision was <5% for Li and B, ~1% for Na, Mg, Mn,
200 and Sr, 20% for Ba, and 10% for U/Ca (2SD) based on the standard with the most similar element/Ca
201 ratio to the samples. However, the concentration of Ba and U in ACC is much higher than these
202 secondary standards, such that this is likely an overestimate of analytical reproducibility. To assess
203 procedural reproducibility, powder splits of five ACC samples were analysed twice. The average
204 difference between the two analyses was 6% for Li, 3% for B, 9% for Na, <2% for Mg, Mn, and Sr, 4%
205 for Ba, and 3% for U/Ca, comparable to the long-term reproducibility of the measurements.

206

207 **2.3 Seawater analysis and speciation calculations**

208 Seawater samples were analysed for their DIC concentration immediately after each experiment to
209 avoid equilibration with the atmosphere using a LI-7000 CO_2 differential, non-dispersive, infrared gas
210 analyser (Apollo SciTech AS-C3). Calibration was performed using a seawater standard (Dickson
211 batch 141), and in-house Na_2CO_3 standards were used to confirm the linearity of the analyser at the
212 relatively high DIC of our experimental seawaters (Evans et al., 2019). The precision of individual
213 samples assessed by repeat (>6) injections was routinely <0.2%, however because the instrument was

214 not calibrated before every sample, we report a conservative estimate of accuracy of $\pm 8\%$ based on the
215 long-term variability in the calibrations.

216

217 Selected seawater samples were analysed for their trace element concentrations on a Thermo Element
218 2 SF-ICPMS at the National Oceanography Centre, Southampton, UK. Samples were diluted 1:500
219 with 3% HNO₃ spiked with 5 ppb In as the internal standard. Calibration was performed via an eight-
220 point calibration line spanning the range of sample concentrations. ⁷Li, ¹¹B, ⁸⁶Sr, ¹³⁸Ba, and ²³⁸U were
221 measured in low resolution mode, whereas ²⁴Mg, ⁴³Ca, ⁴⁴Ca, and ⁵⁵Mn were measured in medium
222 resolution mode. In order to avoid dilution error (if present) impacting the seawater data, sample-
223 specific dilution factors were calculated using the seawater [Ca²⁺], which is 10.3 mM in the case of the
224 reservoir seawaters, and can be calculated in the case of seawaters collected at the end of the
225 experiment using the calibrated Ca ISE as described in Sec. 2.1 (reservoir [TE]_{corrected} = [TE]_{measured} ×
226 [Ca]_{calculated}/[Ca]_{measured}). Precision was assessed based on a pooled standard deviation of repeat analysis
227 of seawater samples from two different reservoirs, to provide an estimate of data quality based on a
228 larger number of analyses. Analytical reproducibility was 6% for Li, 4% for B, 6% for Mn, 6% for Sr,
229 18% for Ba, and 5% for U/Ca, respectively (1SD).

230

231 The Mg/Ca ratio of the seawaters collected at the end of each experiment were determined using the
232 Varian Vista Pro ICP-OES (axial) at the Edinburgh Earth Observatory, UK. Samples were diluted 1:50
233 with 3% HNO₃ with 1 ppm Y as the internal standard. Calibration was performed via a six-point
234 calibration line with a range of Mg and Ca concentrations spanning that of the samples. Precision
235 based on replicate analysis of the seawater reservoirs was 2% (2SD) for Mg/Ca. In order to identify
236 whether seawater Mg/Ca remained constant during the experiments, the calculated Mg/Ca at the
237 onset of precipitation was compared to the measured Mg/Ca ratio at the end of the experiment. These
238 datasets are offset by 1% on average, demonstrating no significant change in seawater Mg/Ca,
239 although individual experiments may be offset from expected values by up to 10%. Given that
240 insufficient ACC was precipitated to significantly change the seawater [Mg] (Fig. S4), we interpret this
241 variance as resulting from a combination of the precision of the Ca ion-selective electrode (ISE) in
242 seawater, the precision of the ICP-OES data, and possible minor precipitation between collection and
243 filtration of the seawater samples at the end of the experiment.

244

245 Over the course of the experiments, CaCl_2 and Na_2CO_3 titration was performed until sufficient
246 precipitate for characterisation had been produced (10-40 mg). In order to assess (1) whether trace
247 element uptake into ACC resulted in a lowering of the seawater concentration, and (2) to ensure no
248 procedural contaminant was present, the composition of seawater at the start and end of six
249 experiments was compared. Variations in the concentrations of all elements between the start and the
250 end of the experiment were broadly comparable to analytical precision (Tab. S4), with the exception of
251 Mn. Seawater [Mn] decreased during all experiments because the ACC D_{Mn} is high (Sec. 3.2), by ~30%
252 on average with individual experiments characterised by a decrease of 8-75% (8-30% excluding one
253 analysis). Our reported D_{Mn} should therefore be considered in the context of a ~20-30% decrease in
254 the seawater [Mn] during the course of the titrations such that these represent a lower constraint of
255 ACC D_{Mn} rather than the true values, and with some of the variance in the D_{Mn} data explicable
256 through changes in [Mn] during titration. In the case of experiments dominantly yielding calcite, the
257 variation in element/Ca ratios over the course of the titration was often much higher (up to 50%)
258 because the dosing rate was typically lower than the precipitation rate in these experiments. The
259 calculated distribution coefficients for these experiments should be viewed in this context (Tab. 1),
260 although we stress that we do not interpret these data, which are presented only to give a sense of the
261 extent to which they differ from ACC precipitated under comparable carbonate system conditions.

262

263 Aqueous speciation modelling and activity calculations were performed with PHREEQC (Parkhurst
264 and Appelo, 1999) v3.6 using both the minteq.v4 and pitzer databases for comparison; minteq
265 considers a wider variety of ion pairs whereas pitzer is more applicable to high ionic strength solutions
266 such as seawater. The exception to the above was boron, for which speciation was calculated using the
267 temperature, salinity, $[\text{Ca}^{2+}]$, and $[\text{Mg}^{2+}]$ dependent pK_B using the MyAMI model of Hain et al. (2015)
268 assuming that $[\text{B}(\text{OH})_3] + [\text{B}(\text{OH})_4^-] = [\text{B}_T]$. While the PHREEQC speciation model indicates that 4-
269 11% of B_T is present as the $\text{CaB}(\text{OH})_4^+$ ion pair (average 6%) and 6-12% is present as the $\text{MgB}(\text{OH})_4^+$
270 ion pair (average 10%), we do not account for this when discussing boron partitioning in order to
271 facilitate direct comparison to the majority of previous studies.

272

273 Note that square brackets are used throughout to denote total concentration, e.g. $[\text{Ca}^{2+}]$ does not
274 imply a speciation calculation has been performed. Activities, free ion concentrations, and speciation
275 calculations are noted where relevant.

276 3. Results

277 3.1 Precipitate characteristics and precipitation dynamics

278 ACC precipitated from seawater is characteristically formed of spherical shaped aggregates of
279 approximately 100 nm diameter (Fig. 1A,B). Raman and FTIR spectra of the majority of the
280 precipitates discussed here display characteristic features of ACC, such as a lack of visible Raman
281 lattice mode vibrations and wide ν_1 peak (carbonate symmetric stretch, see Fig. 1E), as well as ~20
282 weight% water of crystallisation as evidenced by TGA-MS (Evans et al., 2019). Based on spectroscopic
283 features such as these, the lack of any resolvable crystal structure based on XRD data of similar
284 samples (Evans et al., 2019), as well as the geochemical data (see below), the precipitation experiments
285 yielded exclusively ACC in all but two cases. Specifically, those conducted at the extreme basic end of
286 the carbonate chemistry space investigated here resulted in ACC-brucite mixtures, whilst samples
287 precipitated from seawater with a Mg/Ca ratio <1 were calcite or calcite-ACC mixtures (Fig. 1C,D,F,G
288 and the supplementary material).

289
290 The carbonate and seawater chemistry conditions at which precipitation took place are summarised in
291 Fig. 2 and described in detail in Evans et al. (2019). Briefly, in seawater with an initial Mg/Ca ratio
292 close to natural (53/10.3 mM), ACC precipitation takes place when the $[\text{Ca}^{2+}]/[\text{CO}_3^{2-}]$ is close to 1, i.e.
293 $[\text{CO}_3^{2-}] = 10 \pm 2$ mM (Fig. 2A). The addition of amino acids serves to inhibit ACC precipitation, which
294 in our experimental setup is overcome by additional CaCl_2 titration, so that amino acid concentration
295 broadly covaries with the seawater $[\text{Ca}^{2+}]$ at the onset of precipitation. The only investigated method
296 by which we were able to reduce the $[\text{CO}_3^{2-}]$ necessary for precipitation substantially below 10 mM
297 (conditions potentially more relevant to the calcification site of marine organisms), was to reduce the
298 seawater Mg/Ca ratio (Fig. 2C). Nonetheless, we were unable to precipitate ACC within the pH and
299 DIC range thought to characterise the tropical zooxanthellate corals (Allison et al., 2014; McCulloch et
300 al., 2017), and our lowest pH experiments are at the upper end of estimates of the foraminifera
301 calcification site (de Nooijer et al., 2009; Bentov et al., 2009). However, the carbonate chemistry of
302 seawater was not exhaustively varied in tandem with the seawater Mg/Ca ratio, such that ACC
303 precipitation under directly comparable conditions may be possible.

304

305 In all cases highly saturated conditions with respect to CaCO_3 minerals were required, ranging
306 between $[\text{Ca}^{2+}][\text{CO}_3^{2-}]$ products of 100-200 (mM^2), equivalent to Ω_{calcite} of ~30-60. Based on the

307 rhodochrosite K_{sp} of Johnson (1982), all seawaters used here were undersaturated with respect to this
308 mineral. Based on the strontianite and witherite K_{sp} data from Busenberg & Plummer (1984) and
309 Busenberg & Plummer (1986) and Ba^{2+} , Sr^{2+} , and CO_3^{2-} activities derived from the PHREEQC pitzer
310 model as described above, then the seawater solutions of our experiments were undersaturated with
311 respect to witherite ($\Omega_{witherite} = 0.03-0.16$) but oversaturated with respect to strontianite ($\Omega_{strontianite} =$
312 $3.7-19.7$). As such, we cannot exclude the possibility that some Sr was incorporated into the
313 precipitates as strontianite rather than directly into ACC, although we note that the seawaters were far
314 more saturated with respect to $CaCO_3$ which may imply $CaCO_3$ precipitation rates far higher than that
315 of $SrCO_3$, such that it is likely that the Sr/Ca data reported here dominantly represent Sr incorporation
316 into ACC rather than the precipitates reflecting ACC-strontianite mixtures.

317

318 In the pH/DIC experiment, saturation state at the onset of precipitation is negatively correlated with
319 Mg/Ca_{sw} (Fig. 2C), which varied as different degrees of $CaCl_2$ titration were required to induced
320 precipitation. This was not the case in experiments in which the seawater initial Mg/Ca_{sw} was modified
321 by experimental design, which are characterised by an approximately constant saturation state with
322 decreasing Mg/Ca_{sw} .

323

324 **3.2 Precipitate trace element data**

325 Trace element/Ca ratios and apparent distribution coefficients (see Hauzer et al., 2018 for
326 terminology) of the precipitates were calculated as the element/Ca ratio in the solid relative to the
327 respective ratio in seawater ($[X/Ca_{ACC}]/[X/Ca_{sw}]$, where X denotes the total molar concentration of a
328 trace or major element), detailed in Tab. 1 and shown in Fig. 3 as a function of seawater pH, with
329 seawater-precipitate trace element/Ca relationships shown for comparison. We initially report
330 distribution coefficients relative to the total seawater element/Ca ratio for consistency and because we
331 have no *a priori* knowledge of which species are incorporated into ACC. In the discussion, we explore
332 the possibility that certain species are preferentially incorporated and/or partitioned into anion sites,
333 especially in the case of B and U. Data from experiments that yielded calcite or calcite-ACC mixtures
334 are also shown so that comparison may be made to crystalline samples precipitated under broadly
335 similar carbonate chemistry conditions. Of the precipitates with a crystalline component, endmember
336 experiments conducted at the lowest Mg/Ca_{sw} ($\sim 0.7 \text{ mol mol}^{-1}$) are likely almost entirely composed of
337 calcite and enable a sense of the difference between ACC and calcite to be ascertained when

338 precipitating using our experimental design. However, we do not discuss these data in detail because
339 the precise ratio of calcite/ACC in these samples was not determined.

340

341 All ACC samples were thoroughly washed with ethanol prior to analysis (see Methods), however the
342 absence of a minor seawater contaminant cannot be fully excluded. For the majority of the trace
343 element data we report, the presence of minor amounts of seawater cannot significantly bias the data
344 as most of these elements are present at a high concentration in ACC (e.g. Mg, Sr) or a low
345 concentration in seawater (Mn, Ba, U). Li and Na/Ca ratios in any carbonate sample are sensitive to
346 seawater contamination, although we do not observe the slope between Li/Ca and Na/Ca that would
347 be expected if remnant seawater is the principal control on these trace elements ($\sim 1 \times 10^{-4}$, see Fig. S7).

348

349 **Lithium:** The ACC Li distribution coefficient is low ($\sim 10^{-3}$ to 10^{-2}), with the implication that
350 incorporation cannot be governed by the thickness of the diffusive boundary layer, i.e. the [Li] of the
351 seawater layer around the ACC cannot be greatly modified through the process of precipitation, as
352 very little Li is incorporated. ACC D_{Li} is comparable to the upper range reported for calcite (0.7 -
353 10.1×10^{-3} cf. 4×10^{-3} reported in Marriott et al., 2004). In seawater with a Mg/Ca ratio close to natural
354 there is no significant relationship between D_{Li} and pH ($R^2 = 0.33$, $p = 0.07$), or between seawater-
355 precipitate Li/Ca, when these variables are considered in isolation, in contrast to calcite (Okumura
356 and Kitano, 1986; Fuger et al., 2019). The presence of Asp or Glu at any concentration do not
357 resolvably impact Li incorporation into ACC (Fig. 3B,C), and samples precipitated in low-Mg
358 seawater are not offset from the others. Combining all of these experiments, D_{Li} in ACC is $1.3 \pm 0.8 \times 10^{-3}$
359 (2SD). Raising the seawater $[\text{Ca}^{2+}]$ above 20 mM was the only investigated variable to result in an
360 offset from the data described above; these experiments are characterised by more scattered Li/Ca
361 values for a given pH, and a higher D_{Li} up to ~ 0.01 . However, there is no systematic relationship
362 between seawater-ACC Li/Ca (note that the seawater ratio was varied by changing the $[\text{Ca}^{2+}]$), at face
363 value implying a lack of a true D_{Li} for ACC (but see discussion in Sec. 4.1).

364

365 **Boron:** Boron incorporation in ACC is dominantly controlled by the carbonate system (Fig. 3D), as is
366 well-known for the crystalline carbonates (e.g. Uchikawa et al., 2015a; DeCarlo et al., 2018), although
367 the absolute B/Ca of ACC is ~ 2 - $4 \times$ higher than calcite precipitated here and previously reported. The
368 presence of Asp and Glu do not significantly impact ACC B/Ca, and there is also no offset observed in

369 those precipitated from low-Mg seawater. There is also no systematic relationship between ACC and
370 seawater B/Ca (Fig. 3F).

371

372 **Sodium:** The ACC D_{Na} is similar to that of calcite precipitated under similar conditions (Fig. 3H),
373 albeit $\sim 2\times$ higher than calcite and aragonite precipitated from ionically simpler solutions but similar
374 solution Na/Ca ratios (White, 1977; Ishikawa and Ichikuni, 1984). There is no systematic relationship
375 between Na/Ca or D_{Na} with pH or amino acid concentration. Within the variable seawater $[Ca^{2+}]$
376 experiments seawater and precipitate Na/Ca are correlated (Fig. 3I), indicating that there is a Na
377 distribution coefficient into ACC, but the relationship is not statistically significant ($R^2 = 0.64$, $p =$
378 0.06) and the degree of scatter in the Na/Ca and D_{Na} data indicate that other factors impact Na
379 incorporation.

380

381 **Magnesium:** The Mg/Ca ratio of ACC precipitated from seawater with Mg/Ca close to natural is
382 ~ 300 - 400 mmol/mol, ~ 4 - $5\times$ higher than seeded overgrowth calcite precipitation in seawater (Mucci
383 and Morse, 1983) and twice as high as calcite formed from ACC transformation in ionically simpler
384 solutions (Blue et al., 2017). The relationship between seawater and ACC Mg/Ca is nonlinear, being
385 best described by a power relationship:

386
$$Mg/Ca_{ACC} = 183 \pm 21 \times Mg/Ca_{sw}^{0.58 \pm 0.09} \quad (\text{eq. 1})$$

387 $R^2 = 0.80$, $p \ll 0.01$, $RMSE = 44$ mmol mol⁻¹ (coefficient uncertainties are 1SE). ACC is similar to
388 calcite in this respect (Mucci and Morse, 1983), albeit with a marginally higher power coefficient ($H =$
389 0.4 for calcite). There is no relationship between D_{Mg} and pH (Fig. 3K), in contrast to calcite (Burton
390 and Walter, 1991), although ACC precipitated at the extreme basic end of the investigated pH range
391 (>10) are offset to Mg/Ca ratios ~ 100 - 200 mmol/mol higher. This most likely results from a minor
392 brucite component in these samples (Fig. S1), and as such all experiments precipitated at a $pH > 10$ are
393 excluded from further discussion. Both the presence of both Asp and Glu in solution lower the Mg/Ca
394 ratio of ACC (Fig. 3J), with the degree to which this is the case nonlinearly dependent on amino acid
395 concentration (see Sec. 4.2).

396

397 **Manganese:** Mn/Ca in ACC is positively correlated with pH in ACC precipitated from seawater with a
398 Mg/Ca ratio close to natural (D_{Mn} increased with a slope of 27 ± 4 per pH unit, Fig. 3M). Across all
399 experiments, in some of which the $[Mg^{2+}]$ and/or $[Ca^{2+}]$ was varied by experimental design, a much

400 larger range ($D_{Mn} = 20-200$) was observed, similar to or slightly higher than that of calcite (Mucci,
401 1988). Nonetheless, we again stress that we do observe a decrease in the seawater [Mn] during the
402 course of precipitation in our experiments (Sec. 2.2) such that these D_{Mn} are minimum values and
403 some of the variance in the data is likely driven by possible differences in the amount of precipitation
404 that took place between experiments. The addition of both Asp and Glu result in lower ACC Mn/Ca,
405 but in contrast to Mg/Ca, the degree to which this is the case is amino acid dependent. For a given
406 concentration, ACC precipitated in the presence of Asp has a lower Mn/Ca ratio compared to
407 glutamic acid. Increasing the seawater [Ca^{2+}] resulted in higher Mn/Ca, and therefore a much higher
408 D_{Mn} , despite the resulting lower seawater Mn/Ca ratios (Fig. 3M,N). Whilst not apparent from Fig.
409 3M,N,O, unlike most other trace elements, much of the variance in D_{Mn} described above can be
410 explained by the seawater saturation state, discussed in detail in Sec. 4.1.

411

412 **Strontium:** We find no systematic relationship between ACC Sr/Ca and any parameter with the
413 exception of Sr/ Ca_{sw} (Fig. 3R). Unlike all of the other investigated trace elements, ACC-seawater Sr/Ca
414 are linearly related irrespective of the seawater [Mg^{2+}] or amino acid concentration:

$$415 \quad Sr/Ca_{ACC} = 0.67 \pm 0.02 \cdot Sr/Ca_{sw} \quad (\text{eq. 2})$$

416 $R^2 = 0.74$, $p \ll 0.01$, $RMSE = 0.65 \text{ mmol mol}^{-1}$. The ACC D_{Sr} is around three times higher than that of
417 inorganic calcite (Mucci and Morse, 1983), but around half that of inorganic aragonite (Dietzel et al.,
418 2004). The ACC Mg/Ca ratio does not impart a resolvable control on D_{Sr} , in contrast to calcite (Mucci
419 and Morse, 1983), wherein lattice distortion resulting from Mg substitution for Ca is thought to result
420 in increased Sr incorporation.

421

422 **Barium:** Like Sr, Ba/Ca is not characterised by a systematic relationship with pH, with a relatively
423 invariant distribution coefficient of 1.82 ± 0.27 , around $20\times$ higher than calcite (Kitano et al., 1971) but
424 only marginally ($1-2\times$) higher than that of inorganic aragonite (Dietzel et al., 2004; Mavromatis et al.,
425 2018). There is also no systematic relationship between D_{Ba} and amino acid concentration. ACC
426 precipitated from low-Mg seawater (10 mM) has a lower Ba/Ca ratio (Fig. 3T), $D_{Ba} = 0.79 \pm 0.06$.
427 Experiments in high-Ca seawater result in ACC with similar Ba/Ca ratios (Fig. 3U), but higher
428 distribution coefficients (driven by the denominator).

429

430 **Uranium:** Uranium incorporation into ACC is unresolvably impacted by amino acid concentration,
431 seawater $[Mg^{2+}]$, or pH. Considering all three experimental sets together yields a constant D_U of
432 0.13 ± 0.03 (Fig. 3W), with only ACC from the experiments performed in high-Ca seawater offset to
433 higher U/Ca and D_U values. This is lower than inorganic aragonite ($K_U = \sim 0.4$ in the most highly
434 saturated experiments of Decarlo et al. (2015)) but higher than that of calcite ($K_U = 0.05$ in the highest
435 rate experiments of Weremeichik et al. (2017)). In aragonite the $UO_2(CO_3)_3^{4-}$ complex substitutes for
436 $CaCO_3$, in contrast to calcite, wherein incorporation may occur via adsorption at step edges (Reeder et
437 al., 2000; Reeder et al., 2004). ACC K_U alternatively calculated using the seawater U/ CO_3^{2-} ratio reveals
438 a positive relationship with pH in the subset of experiments conducted in seawater with the normal
439 Mg/Ca ratio ($m = 0.040$, $R^2 = 0.78$, $RMSE = 8.7 \times 10^{-3}$). However, we find no relationship between ACC
440 U/Ca and the seawater U/ CO_3^{2-} ratio.

441

442 The results above relate ACC element/Ca ratios to the respective total concentration ratio in seawater.
443 This simple approach ignores that the free ion activity of all of the trace elements considered here is
444 lower than the total concentration, but is useful because taking speciation or activity into account
445 necessarily assumes something about the mechanism of incorporation. The results of the PHREEQC
446 ion activity calculations are shown in Fig. 4 in comparison to the total concentration ratios for all
447 amino acid-free experiments. This exercise demonstrates that total concentration ratios are linearly
448 related to activity ratios in all cases, i.e. the dominant control on the activity ratios in these
449 experimental seawaters is the concentration ratio, driven mostly by changes in $[Ca^{2+}]$. As such,
450 uncertainty over which species are incorporated into ACC, as well as uncertainty in the speciation and
451 activity calculations, cannot result in artefacts in the trends visible in Fig. 3 and in the more detailed
452 discussion below. Calculating ACC (trace) element distribution coefficients using the activity ratios
453 would result in values ~ 3 times higher in the case of Li and Na, whereas Mg/Ca and Sr/Ca activity
454 ratios are not substantially different from their respective concentration ratios, such that the
455 distribution coefficients described above and shown in Fig. 3 are not sensitive to alkali earth metal
456 speciation in seawater. The minteq.v4 and pitzer databases predict α_{Ba}/α_{Ca} ratios that differ by $\sim 50\%$,
457 with the pitzer database, which is more applicable to high ionic strength solutions such as seawater,
458 yielding a Ba/Ca activity ratio that would result in $D_{Ba} \sim 27\%$ lower than the concentration ratio.
459 Mn/Ca activity ratios differ by an order of magnitude using the two databases, with the pitzer database
460 resulting in α_{Mn}/α_{Ca} ratios $\sim 7\%$ lower than the concentration ratio. Considering seawater activity ratios

461 rather than concentration ratios would result in a linear transformation of the data to a good
462 approximation, and would only produce distribution that differ by <10% from those reported in Tab.1
463 except in the case of Li, Na, and Ba.

464

465 **4. Discussion**

466 **4.1 Growth rate and cation co-incorporation**

467 Precipitation rate is an important factor controlling trace element incorporation into the crystalline
468 carbonate minerals via (e.g.) surface entrapment (Watson, 2004; DePaolo, 2011). Whilst it is probable
469 that the same, or related, processes also impart an effect on trace element partitioning between
470 seawater and amorphous calcium carbonate, this is difficult to assess in our experiments because we
471 have no constraint on surface area-normalised ACC growth rate. Within the subset of 16 experiments
472 for which $[Mg^{2+}]$ was held constant at the natural value (53 mM) and no amino acids were added
473 (both factors are likely to influence precipitation rate), there is no relationship between seawater
474 saturation state and apparent distribution coefficient except in the case of D_{Mn} (Fig. S2), either
475 implying that growth rate is not important, that the $[Ca^{2+}][CO_3^{2-}]$ product is not a good proxy for
476 ACC growth rate, or that some other factor must also be considered. An argument against the first
477 two of these considerations is that there is a negative relationship between D_{Mn} and $[Ca^{2+}][CO_3^{2-}]$
478 which is also known for calcite (Mucci, 1988), implying that growth rate considerations are applicable
479 to ACC but masked by an additional factor in the case of Li, Ba, and U. Prime candidates are
480 competition between cations for incorporation into ACC, or that the composition of ACC itself may
481 impact the incorporation of other trace elements. For example, in the case of calcite, Mg substitution-
482 induced lattice distortion increases D_{Sr} (Mucci and Morse, 1983; Evans et al., 2015). Whilst a directly
483 analogous process cannot exist in amorphous materials, ACC has short-range order which is impacted
484 by its Mg/Ca ratio (Lam et al., 2007), and/or it may be that trace element distribution coefficients into
485 ACC are best described as the ratio to Ca+Mg given the overall high ACC Mg/Ca ratios (see the
486 supplementary material for an exploration of this). In either case the precipitate or seawater Mg/Ca
487 ratio could be an important consideration. There is no significant relationship between ACC Mg/Ca
488 and D_{Sr} (Fig. 5A), in contrast to calcite, whereas there is a strong effect of Mg/Ca on D_{Ba} (Fig. 5B). This
489 lends support either to the ACC Mg/Ca ratio imparting a control on the incorporation of some low
490 concentration trace elements for structural reasons, or to the notion that molar ratios in high-Mg
491 samples should be reported with Mg+Ca as the denominator (Fig. S7).

492

493 Given that both growth rate and the seawater or ACC Mg/Ca ratio are important controls on the
494 incorporation of at least some low-concentration trace elements, multiple linear regression (MLR)
495 analysis were performed on the 16 experiments at constant $[Mg^{2+}]$. As Mg/Ca in seawater and ACC
496 are proportional to one another (Fig. 3L), we account for the possible impact of both seawater and
497 precipitate Mg/Ca using the ACC Mg/Ca ratio using regressions of the form:

$$498 \quad D_x = c + m_1 \cdot Mg/Ca_{ACC} + m_2 \cdot ([Ca^{2+}][CO_3^{2-}]) \quad (\text{eq. 3})$$

499 Which assumes that seawater-ACC trace element/Ca ratios are linearly related through the origin.

500 Regression models were produced for Li, Mn, Ba, U, the four trace elements for which there is clearly
501 more than one dominant control on their incorporation into ACC (Fig. 3C,O,U,X). All four models
502 are highly significant; R^2 range between 0.73-0.84, $p < 0.01$, RMSE/intercept ratios = 4-5% (Tab. S1),
503 implying that these trace elements do in fact have an approximately linear distribution coefficient in
504 ACC, overprinted in our experiments by the effect of ACC Mg/Ca and seawater saturation state. Both
505 of these secondary factors are significant predictors in all models except in the case of D_{Mn} , which can
506 be well-modelled by saturation state alone. That is, most of the variance in the observed trace
507 element/Ca ratios can be ascribed to some combination of the seawater element/Ca ratio, saturation
508 state, and the seawater or ACC Mg/Ca ratio. Whilst this also suggests ACC growth rate is linked to
509 saturation state we stress that, in the absence of direct observational evidence for this, a causal link
510 between saturation state and trace element incorporation via a presumed growth rate effect should be
511 interpreted with caution.

512

513 If the saturation state effect predicted by these models is best attributed to growth rate, then an
514 alternative formulation of this factor might be appropriate given that, in the case of calcite, growth
515 rate is a function of the solution $[Ca^{2+}]/[CO_3^{2-}]$ ratio at constant Ω_c (Nehrke et al., 2007; Wolthers et
516 al., 2012). In order to explore this, we repeat the MLR exercise with the saturation state parameter
517 alternatively formulated as $[Ca^{2+}][CO_3^{2-}]/([Ca^{2+}]+[CO_3^{2-}])$. This accounts for an imbalanced
518 $[Ca^{2+}]/[CO_3^{2-}]$ ratio in the denominator and is therefore more likely to be representative of growth rate
519 (e.g. at constant Ω , 2+50 mM is larger than 10+10 mM, in-line with lower rates at ratios further from
520 unity). These models result in slightly better fits to the data (RMSE reduced by ~15-40% compared to
521 Eq. 3) and result in greater importance being assigned to this metric of growth rate and less
522 importance to the ACC Mg/Ca ratio as predictors of D_x (see the supplementary material). This

523 suggests that the $[Ca^{2+}] [CO_3^{2-}]$ product/sum ratio may be a better metric for growth rate where this
524 cannot be readily independently assessed (e.g. via surface area measurement). For the purposes of the
525 discussion here, it stands that some combination of saturation state/rate, Mg/Ca, and seawater
526 element/Ca ratio results in model RMSE similar in magnitude to analytical precision, however the
527 MLR models are formulated.

528

529 Pertinently, the MLR analysis of D_U is better able to explain the dataset when D_U is formulated relative
530 to U/Ca_{sw} rather than the U/CO_3^{2-} ratio. This points towards an ACC U incorporation mechanism
531 wherein $UO_2(CO_3)_3^{4-}$ is not the only species incorporated into ACC, in contrast to aragonite (Reeder
532 et al., 2000). Alternatively, it may be that the majority of U_T is in the form of $UO_2(CO_3)_3^{4-}$ in all of our
533 experiments such that the exact seawater $[CO_3^{2-}]$ exerts little control on the concentration of the
534 $UO_2(CO_3)_3^{4-}$ complex (see Keul et al., 2013). Whilst the latter hypothesis can explain the poorer
535 performance of the D_U model that uses seawater U/CO_3^{2-} , it cannot explain the better performance of
536 the model utilising U/Ca_{sw} . Like the other trace elements discussed above, ACC D_U is clearly tightly
537 related to seawater chemistry in our experiments, although further work is required to better
538 understand the exact mechanism of incorporation.

539

540 The range of ACC D_x are summarised in Fig. 6 and compared to selected published calcite data
541 (Kitano et al., 1971; White, 1978; Mucci and Morse, 1983; Okumura and Kitano, 1986; Mucci, 1988;
542 Marriott et al., 2004; Uchikawa et al., 2015; Weremeichik et al., 2017). ACC trace element distribution
543 coefficients are 5-100 times higher than in calcite on average, with the exception of D_{Mn} , which is
544 similar in both materials, and D_{Li} , for which the upper end of the calcite range overlaps with ACC. As
545 with our ACC samples, a wide range in calcite distribution coefficients have been reported, driven by
546 factors such as precipitation rate and the Mg/Ca ratio of the solid phase. Therefore, the size of the
547 boxes in Fig. 6 represents the observed variance in distribution coefficients driven by environmental
548 parameters, not uncertainty in the comparison. Moreover, it is likely that many of these factors drive
549 both ACC and calcite distribution coefficients in the same direction. For example, increasing the
550 $[B(OH)_4^-]/DIC$ ratio results in higher B/Ca ratios in both materials. The intersection of the fields in
551 Fig. 6B with the 1:1 line do not imply that the calcite and ACC distribution coefficients are within
552 range of each other.

553

554 4.2 Factors affecting boron and magnesium incorporation into ACC

555 In Sec. 4.1 (and Fig. 3) we demonstrate that Sr and the low concentration trace elements have an
556 approximately constant distribution coefficient into ACC, which may be modulated by the seawater
557 and/or ACC Mg/Ca ratio, and seawater saturation state. Here we examine the controls on B and Mg
558 incorporation in detail given their importance as proxy systems and because their incorporation is
559 also dependent on other factors beyond those discussed above.

560

561 **Boron:** ACC B/Ca principally depends on seawater pH (Fig. 7A), irrespective of the seawater $[Mg^{2+}]$,
562 $[Ca^{2+}]$, or amino acid concentration. At face value, this suggests that the incorporation mechanism of
563 boron into ACC is relatively simple. If it is the negatively charged $B(OH)_4^-$ that is incorporated into
564 ACC, then the mechanistic basis for this relationship should be rooted in the pH-dependent seawater
565 $[B(OH)_4^-]$ or $[B(OH)_4^-]/DIC$ ratio (or similar, e.g. $[B(OH)_4^-]/[HCO_3^-+CO_3^{2-}]$), as previously observed
566 for calcite and aragonite (Uchikawa et al., 2015; Holcomb et al., 2016). This is indeed the case for
567 experiments precipitated from seawater with a Mg/Ca ratio close to natural (Fig. 7B), yet because
568 increasing the seawater $[Ca^{2+}]$ enabled ACC precipitation at a greatly reduced DIC and $[CO_3^{2-}]$, the
569 variable seawater $[Ca^{2+}]$ experiments do not conform to a B/Ca- $[B(OH)_4^-]/DIC$ relationship.
570 Assuming both $B(OH)_3$ and $B(OH)_4^-$ are incorporated into ACC – i.e. regressing against the total
571 seawater boron (B_T)/DIC ratio – yields a similar result (Fig. 7C), again because the total boron
572 concentration was held constant whilst DIC was reduced in the elevated $[Ca^{2+}]$ experiments. For a
573 similar reason we are not able to identify which boron species (or combination thereof) are
574 incorporated into ACC, because pH and DIC unavoidably covaried in the carbonate chemistry
575 experiments (Fig. 2). That is, the tight relationship between ACC B/Ca and $[B(OH)_4^-]/DIC$ (Fig. 7B)
576 could be driven either by increasing $[B(OH)_4^-]$ and/or decreasing DIC relative to B_T . The relatively
577 narrow range in $[CO_3^{2-}]$ between the experiments in seawater with the natural Mg/Ca ratio (Fig. 2)
578 means that whilst the $B(OH)_4^-/CO_3^{2-}$ ratio might be an additional driver of ACC B/Ca, it cannot be an
579 alternative explanation for the relationships shown in Fig. 7 (Fig. S5). Likewise, $B(OH)_4^-$ activity is
580 directly proportional to $[B(OH)_4^-]$ calculated assuming the sum of the two major boron species in
581 seawater equals $[B_T]$ (which is how the data are displayed in Fig. 7, see Sec. 2.3), with $\gamma_{B(OH)_4^-} = 0.32$.
582 While the abundance of the $CaB(OH)_4^+$ and $MgB(OH)_4^+$ ion pairs do vary in seawaters with
583 manipulated $[Ca^{2+}]$ or $[Mg^{2+}]$ (Fig. S6, $\gamma_{B(OH)_4^-}$ ranges between 0.26-0.39), the magnitude of this effect is
584 far too small to drive the trends discussed above (see Fig. S6).

585 An alternative possibility is that ACC B/Ca could be driven by the seawater $[B(OH)_4^-]$ alone, given
586 that ACC precipitated from seawater with an elevated $[Ca^{2+}]$ lie on the same pH-B/Ca line as all other
587 experiments (Fig. 7A), i.e. the discrepancy described above could be an artefact of normalisation to
588 DIC. However, the asymptote of the seawater $[B(OH)_4^-]$ -pH curve is approached above pH ~ 9.5 , yet
589 there is no reduction in the slope of the B/Ca-pH relationship above this pH. As such ACC B/Ca is not
590 correlated with $[B(OH)_4^-]$ above pH ~ 9.5 , and so $[B(OH)_4^-]$ alone also cannot explain the data. One
591 solution to this issue is to regress the B/Ca data against $[B(OH)_4^-]/DIC$ further normalised to the
592 seawater $[Ca^{2+}]$ (Fig. 7D). Doing so causes B/Ca to collapse onto a single slope, albeit with a reduced
593 goodness of fit compared to the B/Ca- $[B(OH)_4^-]/DIC$ regression through the samples precipitated
594 with a seawater $[Ca^{2+}]$ close to natural (RMSE = 116 and 95 respectively), although this is in-line with
595 the relatively large x -axis uncertainties from the propagated Ca, DIC, and pH estimations. Because the
596 seawater saturation state did not scale with seawater $[Ca^{2+}]$ (as increasing $[Ca^{2+}]$ resulted in a broadly
597 proportionally lower $[CO_3^{2-}]$ required for precipitation, Fig. 2C), this normalisation is not necessarily
598 a growth rate correction (see discussion of saturation state versus the $[Ca^{2+}][CO_3^{2-}]$ product/sum ratio
599 as metrics of growth rate in Sec. 4.1). Fully resolving the mechanistic basis for boron incorporation
600 into ACC is beyond the scope of this study, with possible additional considerations being a change in
601 the characteristics of the growing ACC surface (Branson, 2018), or complex formation between Ca^{2+}
602 and $B(OH)_4^-$ at high calcium concentrations. In any case it is encouraging for boron-based proxies
603 that B incorporation into ACC is strongly sensitive to seawater carbonate chemistry (Fig. 7A), such
604 that precipitation through an amorphous precursor is not necessarily a complication for boron-based
605 proxies.

606

607 **Magnesium:** ACC Mg/Ca is predominantly, nonlinearly, controlled by the seawater Mg/Ca ratio.
608 Figure 7 compares our Mg/Ca data to ACC precipitated at higher Mg/Ca ratios from non-seawater
609 solutions (Blue and Dove, 2015), calcite precipitated from seawater (Mucci and Morse, 1983) and
610 calcite formed from the transformation of ACC (Blue et al., 2017). Our data are in agreement with
611 previous work in that we find ACC Mg/Ca far exceeds that of calcite precipitated under an equivalent
612 Mg/Ca ratio (Blue and Dove, 2015). However, unlike Blue and Dove (2015) we find no resolvable pH
613 dependency of ACC Mg/Ca (Fig. 3K). The reasons for this may stem from the different experimental
614 design, most notably that we precipitate ACC from seawater rather than $MgCl_2$ - $CaCl_2$ - $NaHCO_3$
615 solutions. Whatever the cause for the pH dependency that has been previously reported, our results

616 indicate that it may not be manifest when precipitating from seawater, especially at biologically
617 relevant pH.

618

619 As previously described (Wang et al., 2009), the presence of high concentrations of carboxylated
620 molecules that form ligands with Ca and Mg in solution can impact the Mg/Ca ratio of ACC. The
621 basis for this lies in the differential affinity that these molecules have to form ligands with Mg^{2+} and
622 Ca^{2+} , thereby impacting the free Mg^{2+}/Ca^{2+} ratio. Precipitation in the presence of molecules such as
623 Asp should result in a lower ACC Mg/Ca ratio, as this molecule has a preferential affinity to form
624 ligands with Mg^{2+} over Ca^{2+} in solution. Consistent with this model, we find that ACC precipitation
625 from seawater containing Asp and Glu results in a lower ACC Mg/Ca (Fig. 9) according to a power
626 relationship, with the effect of Asp and Glu being indistinguishable from one another. Increasing the
627 concentration between 2 to 10 mM resulted in ACC with a Mg/Ca ratio ~40% lower than the average
628 of the amino acid-free experiments (290 cf. 425 $mmol\ mol^{-1}$; Fig. 9), whilst further increase up to an
629 amino acid concentration of 40 mM resulted in only a minor further reduction in ACC Mg/Ca to 240
630 $mmol\ mol^{-1}$. This is in contrast to the results of Wang et al. (2009), wherein ACC precipitated in the
631 presence of Asp had a higher Mg/Ca ratio than the biomolecule free control experiment, possibly
632 pointing an additional complicating factor in those experiments. Moreover, the data of Wang et al.
633 (2009) are characterised by a positive relationship between amino acid concentration and ACC
634 Mg/Ca ratio, in contrast to our results and despite the preferential affinity of these molecules to form
635 ligands with Mg^{2+} . One key difference between Wang et al. (2009) and this study is that our samples
636 were precipitated from seawater under tightly controlled carbonate system conditions, such that it
637 may be that ion-pairing and formation of ligands in more complicated solutions such as seawater
638 alters the resulting chemical characteristics of ACC. Whatever the cause, this difference highlights the
639 importance of precipitating ACC under conditions that are as relevant as possible to the system of
640 interest.

641

642 **5. Conclusion**

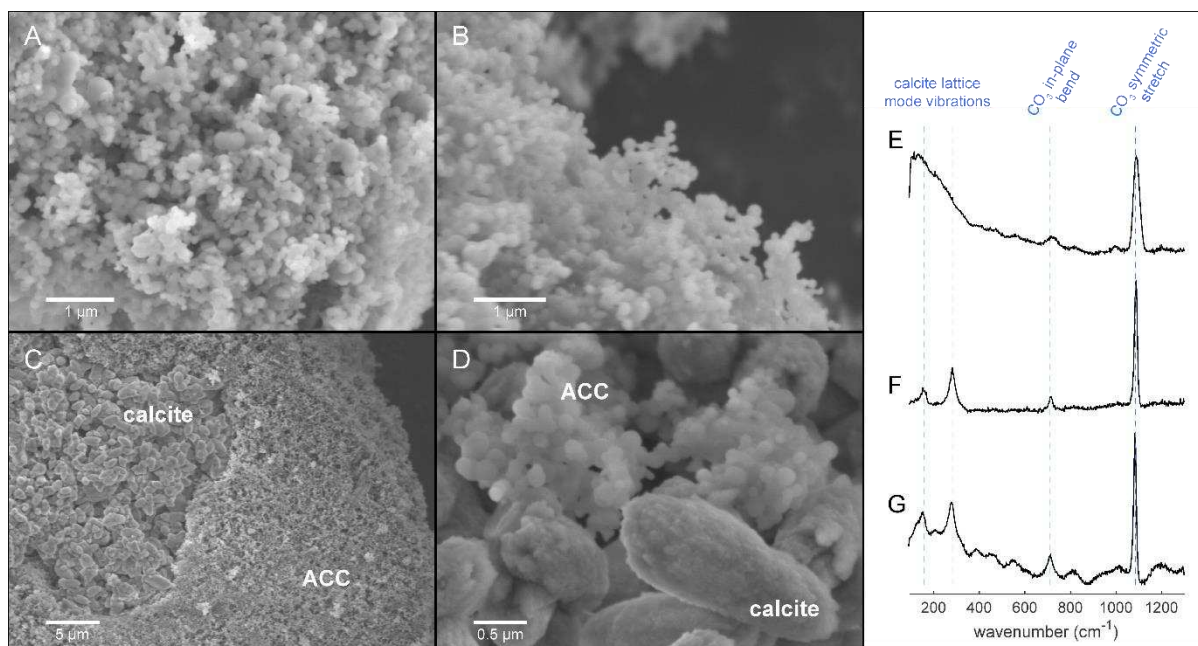
643 The systematics of trace element partitioning between seawater and ACC were investigated under a
644 variety of different carbonate system conditions and element/Ca seawater ratios (principally by
645 varying $[Ca^{2+}]$). Data for many of the most commonly studied trace elements with respect to proxy
646 systems in biogenic carbonate archives and biomineralisation models are presented (Li, B, Na, Mg,

647 Mn, Sr, Ba, U). Several aspects of trace element incorporation into ACC are similar to the seawater-
648 calcite system, e.g. B/Ca is strongly a function of the carbonate system, the seawater-ACC Mg/Ca
649 response is characterised by a power relationship, and Sr has an approximately constant distribution
650 coefficient. In general, trace elements characterised by distribution coefficients lower than one in
651 calcite also have $D_x < 1$ in ACC, although Ba is an exception, and the D_x of all trace elements is ~1-2
652 order of magnitude higher in ACC than calcite, with the exception of Mn (similar for both materials).
653 Unlike calcite, where the solid Mg/Ca ratio imparts a control on D_{Sr} , probably through lattice
654 distortion, there is no relationship between ACC Mg/Ca and D_{Sr} . D_{Ba} is negatively correlated with the
655 ACC Mg/Ca ratio, possibly suggesting that low concentration divalent ions are incorporated to a
656 higher degree when ACC contains less Mg, or that trace element ratios should be reported relative to
657 Mg+Ca in high-Mg samples. Finally, we find that high concentrations (>5 mM) of both Asp and Glu
658 strongly inhibit Mg incorporation into ACC, in contrast with a previous study but as predicted by
659 changes in the Mg/Ca activity ratio as a result of the differential binding constants these organic
660 molecules have to form ligands with Mg^{2+} and Ca^{2+} in solution. The only other trace element
661 resolvably impacted by these amino acids was Mn, with ACC precipitated in the presence of both Asp
662 and Glu characterised by lower D_{Mn} .

663

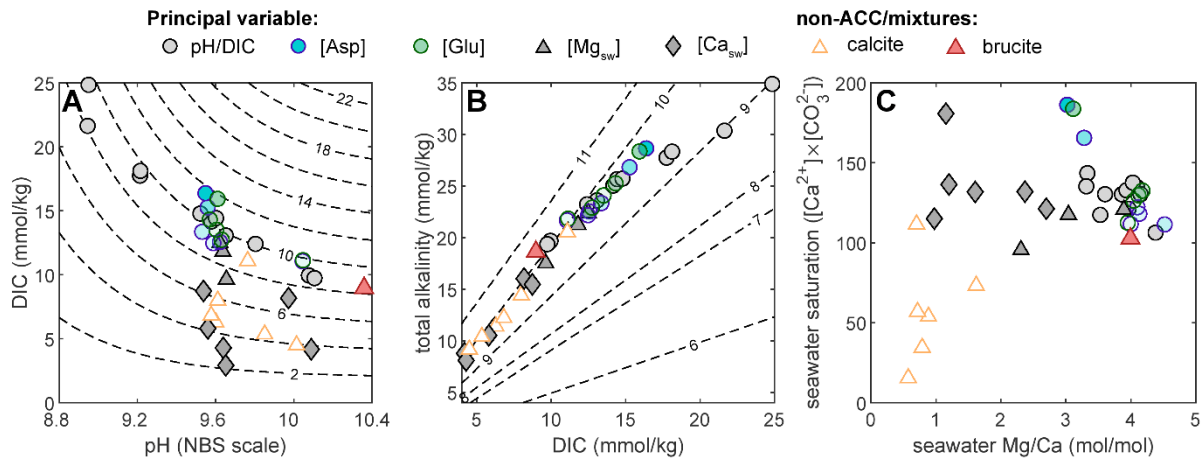
664

665 **Acknowledgments.** We are grateful to Laetitia Pichevin and Matthew Cooper for help with the
666 seawater ICP-OES and ICP-MS analyses, respectively, and we are indebted to Jonathan Erez for many
667 stimulating discussions. We would like to sincerely thank the editor and three anonymous reviewers
668 whose comments substantially improved this contribution. This work was supported by the
669 Leverhulme Trust (Research Project Grant 2015-268 to NA, RK, and KP).



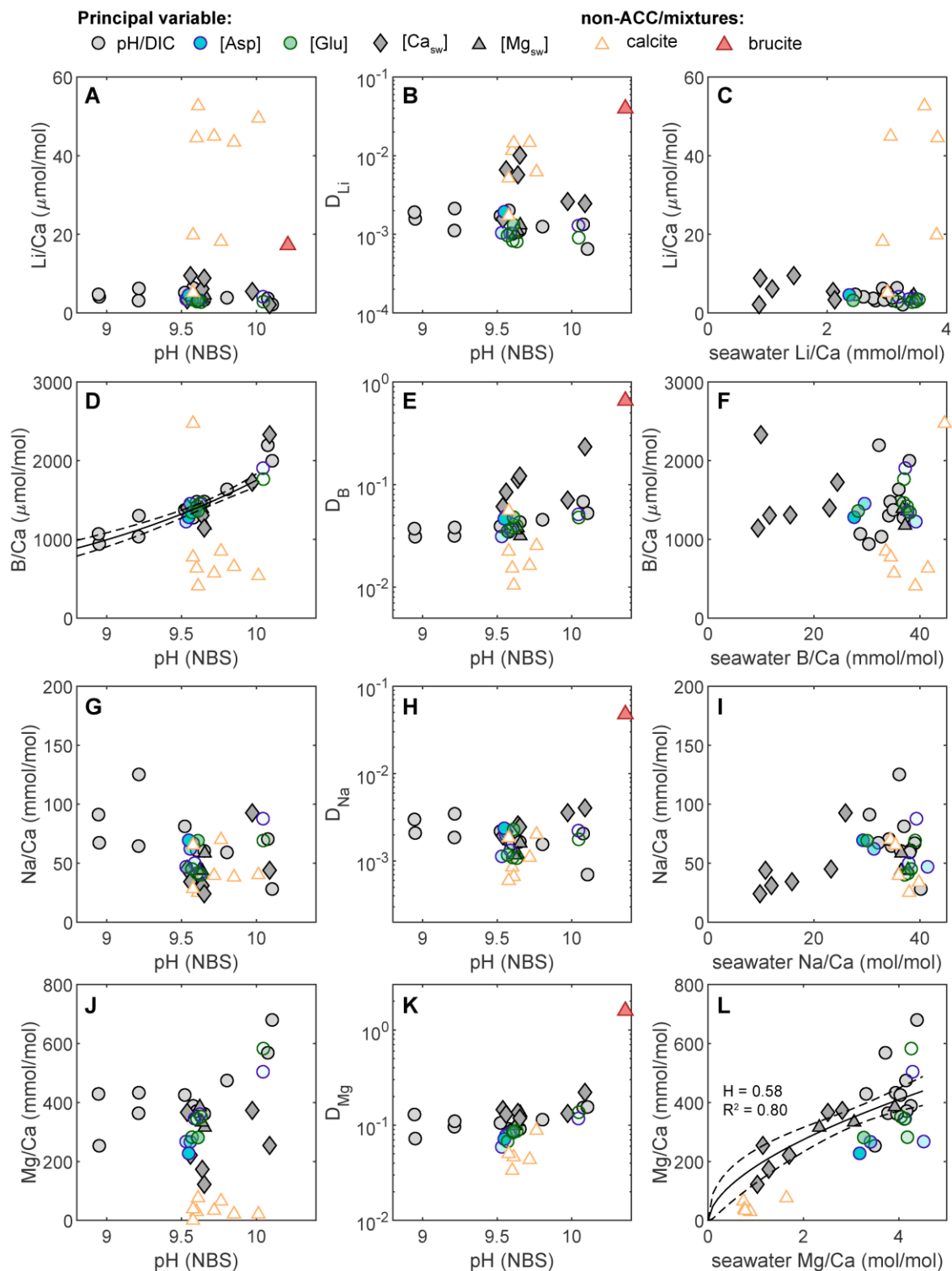
670
671
672
673
674
675
676
677
678
679
680
681
682
683
684
685

Fig. 1. Representative SEM images (A-D) and Raman spectra (E-G) of the precipitates discussed here. (A) ACC precipitated from seawater with the natural Mg/Ca ratio of 5 at pH ~10. (B) ACC precipitated from low-Mg seawater (15 mM) at pH ~9.5. (C) Precipitate resulting from seawater with $[Ca^{2+}]$ increased to result in $Mg/Ca_{sw} < 1$ at pH ~9.5. Two distinct components are present, ACC and calcite (identified through Raman and FTIR spectroscopy). (D) As in panel C except precipitated at pH ~10. Crystalline $CaCO_3$ particles are evident. Note panels C & D are shown for illustrative purposes, calcite was not detectable in most precipitates. (E) Representative Raman spectra of ACC precipitated from seawater with the natural Mg/Ca ratio. The lack of discernible lattice-mode vibrations and the wide ν_1 peak (CO_3 symmetric stretch) demonstrate the amorphous nature of this material (also see Fig. S1). (F) Raman spectra of the precipitate resulting from seawater with a Mg/Ca ratio < 1 at pH 9.5. Lattice-mode vibrations indicate the presence of calcite, whilst the asymmetric ν_1 peak is consistent with the presence of both calcite and ACC (Evans et al., 2019) as also observed via SEM imaging. (G) At $Mg/Ca_{sw} < 1$ and pH 10 calcite lattice-mode vibrations are visible albeit less well-defined, again indicating the presence of both ACC and calcite.



686
687

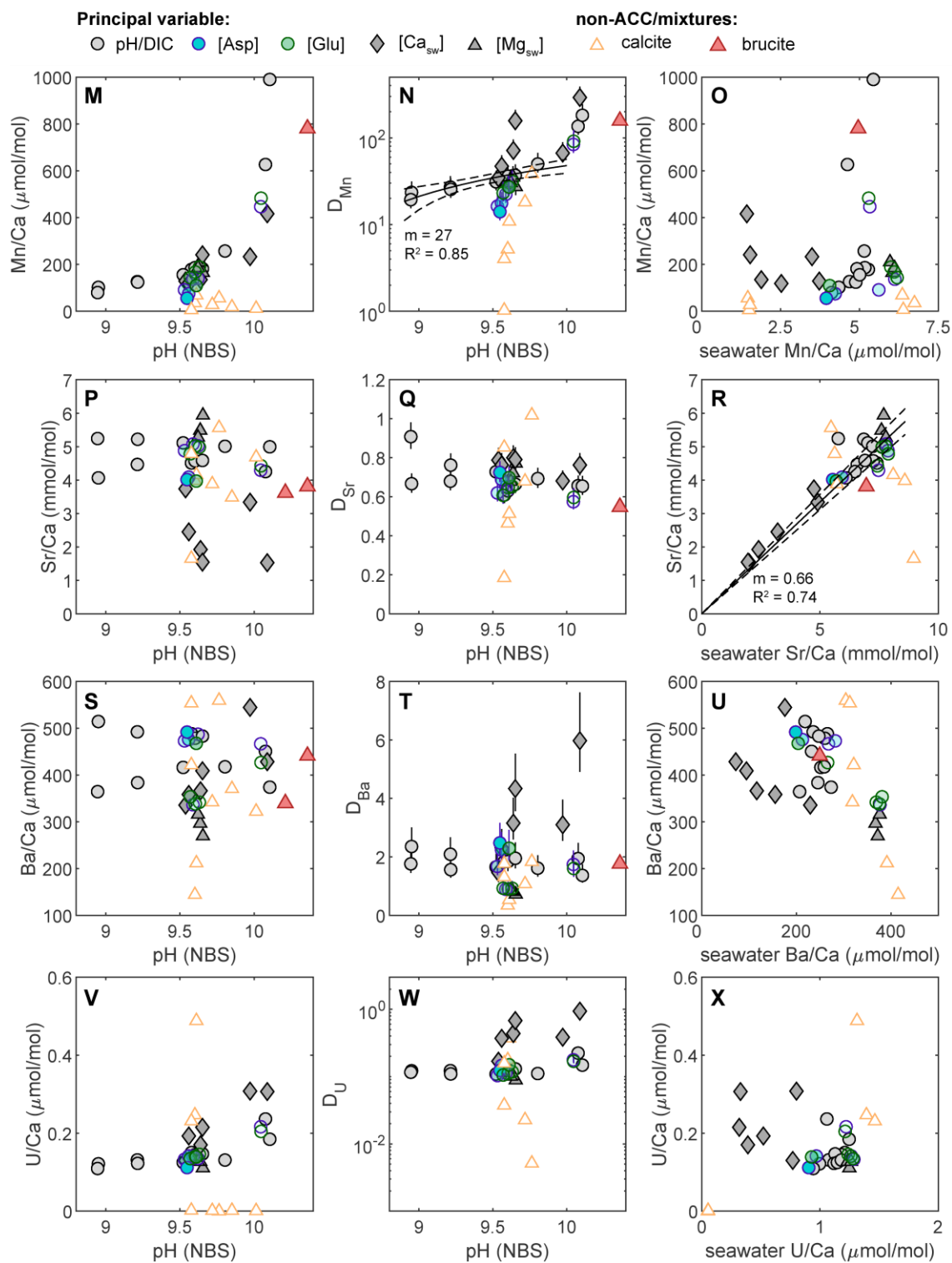
688 **Fig. 2.** The seawater chemistry conditions under which ACC and other materials were precipitated. (A) pH-DIC
689 with $[CO_3^{2-}]$ shown by contours. ACCs precipitated from seawater with Mg/Ca close to the natural ratio of ~5
690 (circles) all fall within ± 2 mM of the 10 mM $[CO_3^{2-}]$ line. Reducing Mg/ Ca_{sw} either through lowering Mg^{2+} or
691 raising Ca^{2+} was the only mechanism investigated here by which the seawater DIC necessary for ACC
692 precipitation could be substantially reduced. Amino acid concentration is shown as a function of symbol opacity
693 (solid colours represent the highest concentration, 40 mM). (B) The location of the experiments in alkalinity-
694 DIC space, with pH shown by contours. (C) The seawater carbonate mineral saturation state ($[Ca^{2+}][CO_3^{2-}]$) at
695 the onset of precipitation as a function of the seawater Mg/Ca ratio. In most cases the resulting precipitate was
696 ACC, with the exception of (1) seawater with a Mg/Ca ratio ≤ 1 mol/mol, which resulted in calcite or calcite-
697 ACC mixtures (see Fig. 1), and (2) at the extreme basic end of the pH range investigated (>10), which resulted in
698 ACC-amorphous brucite mixtures. $[CO_3^{2-}]$ and total alkalinity were calculated from pH and DIC using co2sys
699 (Lewis and Wallace, 1998).



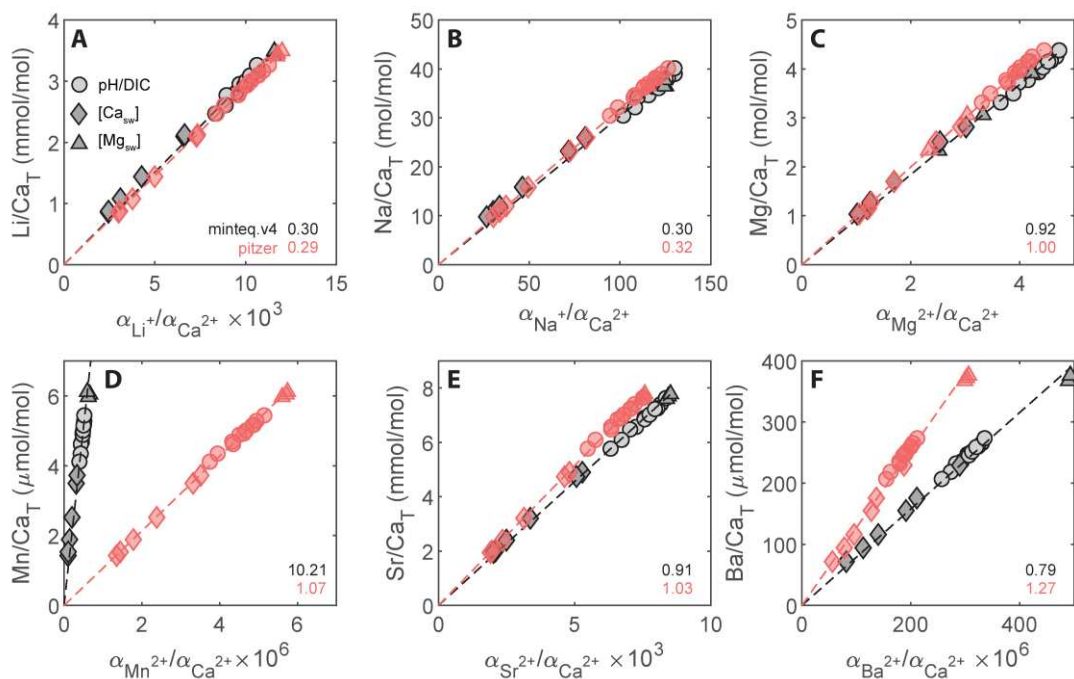
700
 701

702 **Fig. 3.** Overview of trace and major element incorporation into ACC precipitated from seawater as a function of
 703 pH (left, centre) and the seawater element/Ca ratio (right). In the case of pH, both the precipitate element/Ca
 704 ratio (left) and distribution coefficient (centre) are shown as the method used to precipitate ACC meant that the
 705 seawater [Ca²⁺] was not identical in all cases (see methods). Calcites and/or calcite-ACC mixtures precipitated
 706 under similar carbonate chemistry conditions and an amorphous brucite-ACC mixture are shown for
 707 comparison. Note that the latter is omitted from some plots to avoid scale compression, and that the scatter in
 708 the ‘calcite’ data arises because some samples are calcite and some are mixtures based on their Raman spectra.

709 See Fig. S7 for the data replotted as the ratio to Ca+Mg, in order to account for the high mole% Mg of these
 710 ACCs,



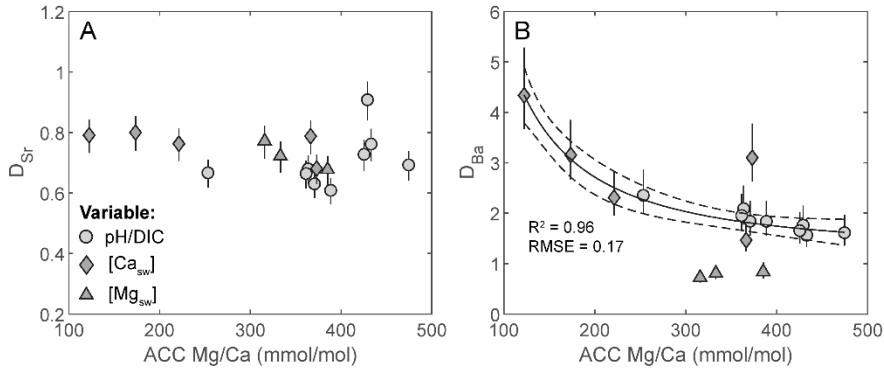
711
 712
 713 **Fig. 3. Cont.**
 714



716

717

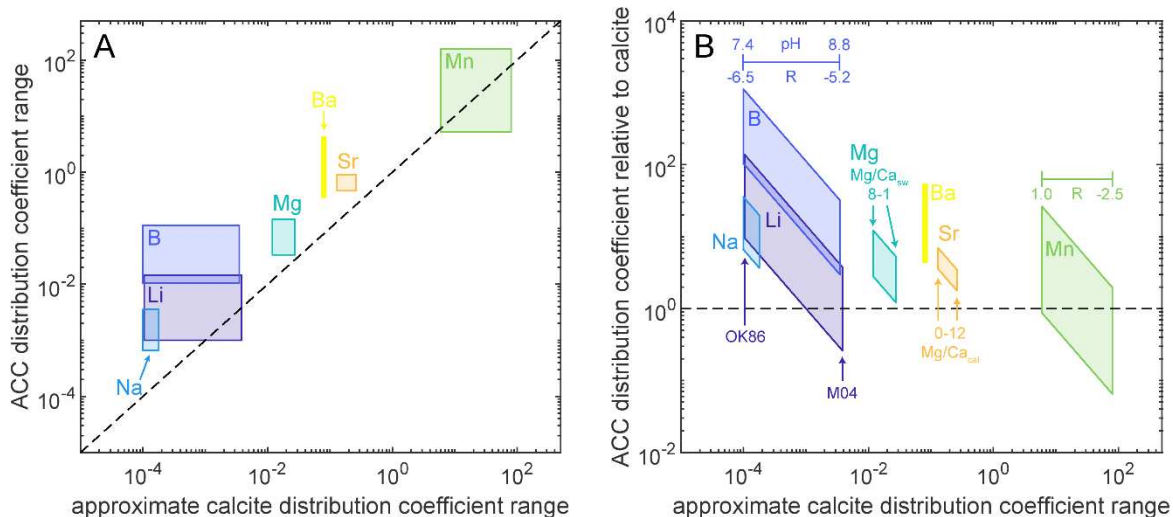
718 **Fig. 4.** The relationship between the ion activity ratios and total concentration ratios for the amino acid-free
 719 experiments presented here, calculated using PHREEQC with both the minteq.v4 and pitzer databases. We note
 720 that the application of the minteq.v4 database to high ionic strength solutions is not necessarily recommended
 721 and is presented here only for comparison. Importantly, the activity-concentration ratio relationship is linear to
 722 a good approximation (slopes given in the lower left corner of each panel), that is, changes in the activity ratio
 723 are principally driven by changes in $[Ca]$ rather than pH, DIC, etc.



724
725

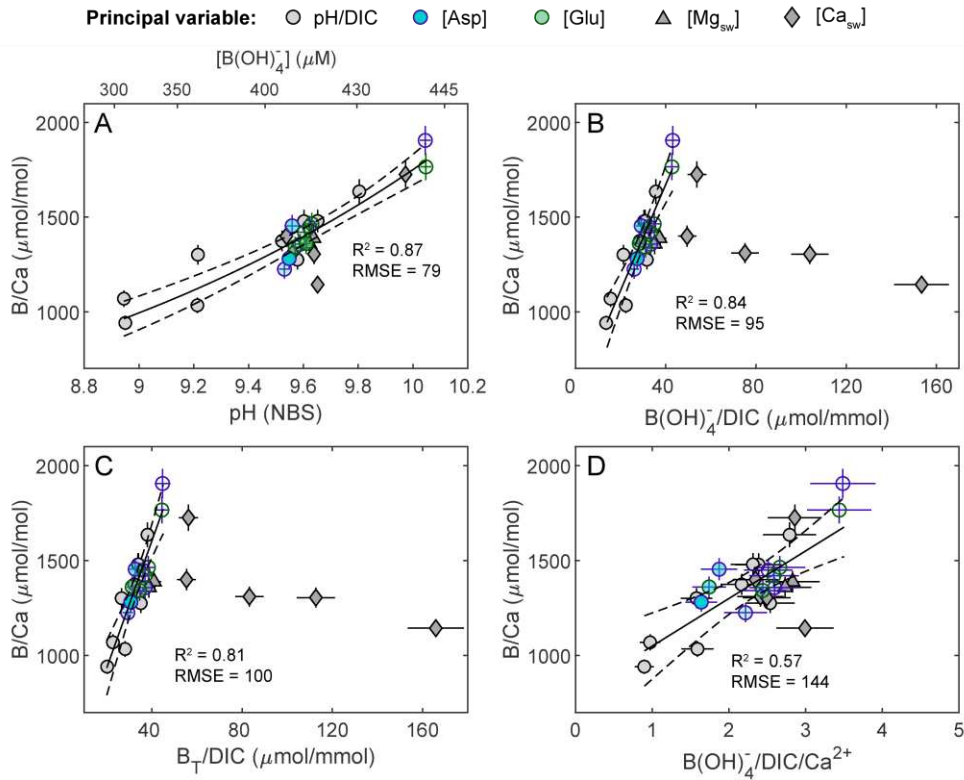
726 **Fig. 5.** Investigating the role of seawater and/or ACC Mg/Ca on the co-incorporation of other alkali earth
 727 metals. (A) There is no relationship between ACC Mg/Ca and D_{Sr} , differentiating ACC from calcite in this
 728 respect (Mucci and Morse, 1983). (B) In contrast, Mg/Ca may exert a strong control on D_{Ba} , possibly implying
 729 competition between Mg^{2+} and the low-concentration divalent metal ions. One outlier (based on its Cook's
 730 distance), and the low-Mg seawater data are excluded from the regression. The overall nonconformity of these
 731 latter data, and the factor of two lower D_{Ba} in low-Mg seawater implies that both seawater and precipitate major
 732 ion chemistry influence ACC Ba incorporation.

733



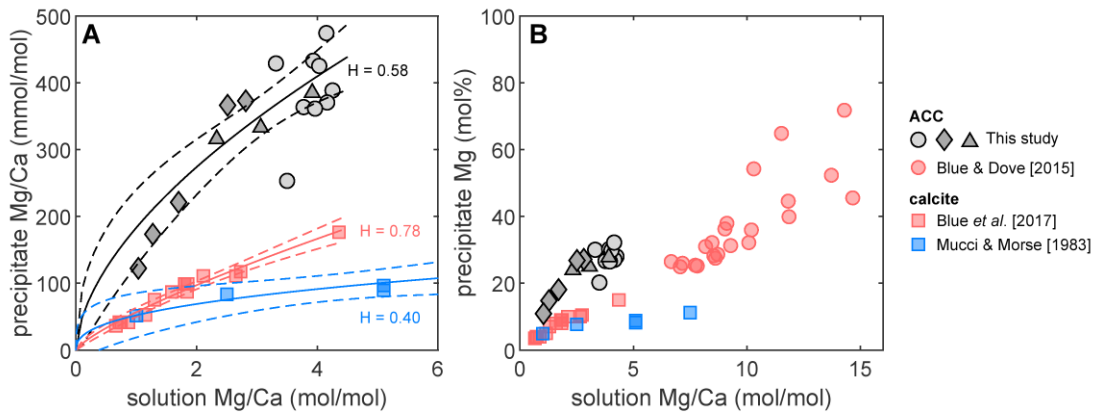
734
735

736 **Fig. 6.** (A) Major and trace element distribution coefficients in ACC precipitated from seawater (this study)
 737 compared to calcite. The heights of the boxes are equal to the range of ACC distribution coefficients found
 738 under the different seawater chemistries investigated here, which is an indication of the extent to which the
 739 distribution coefficient depends on boundary conditions and not an estimate of uncertainty. The widths of the
 740 boxes represent the range of distribution coefficients either within or between calcite studies (more than one
 741 study has been conducted in the case of Li and Na). Where possible, only data from calcite experimentally
 742 precipitated in seawater were used (Mg, Sr only). Note that (e.g.) the narrow width of the Ba box may reflect the
 743 limited amount of research on Ba incorporation into calcite. (B) The ACC distribution coefficients alternatively
 744 displayed relative to the respective calcite values. In general, ACC trace element distribution coefficients are ~5-
 745 100 times higher than calcite with the exception of Mn (but note that we constrain the minimum ACC D_{Mn} of
 746 the experiments presented here, true values may be ~30% higher, see Sec. 2.2). The principal experimental
 747 variables of the calcite studies (growth rate, pH, Mg/Ca_{sw}), or the location of certain studies (in the case of Li) are
 748 labelled. Note that processes that result in a change in the calcite distribution coefficient for a certain trace
 749 element may exert a similar control on the respective ACC distribution coefficient, e.g. increasing pH results in
 750 higher B/Ca ratios in both calcite and ACC. In these cases, the data would be more appropriately displayed using
 751 a (sub)horizontal line, but we do not do so in the absence of directly comparable calcite and ACC experiments
 752 in terms of solution chemistry and experimental design. OK86 and M04 refers to Okumura and Kitano (1986) and
 753 Marriott et al. (2004) respectively, see Sec. 3.2 for other references.
 754



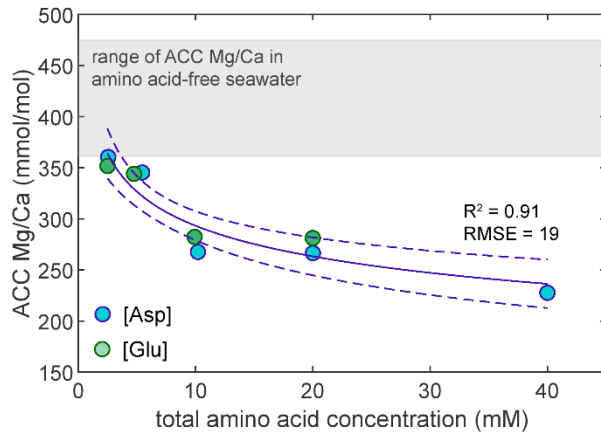
755
756

757 **Fig. 7.** Boron partitioning into ACC. Only data from precipitates which were unambiguously entirely ACC are
 758 shown (see text). (A) B/Ca as a function of pH. (B) B/Ca as a function of the seawater $B(OH)_4^-/DIC$ ratio.
 759 $B(OH)_4^-/DIC$ calculated using DIC measured at the end of precipitation is shown (Tab. S4), except in the case of
 760 the variable [Ca] and [Mg] experiments for which calculated DIC was used (Tab. 1), see Evans et al. (2019). (C)
 761 B/Ca as a function of the seawater total boron/DIC ratio. Although ACC B/Ca is marginally better described by
 762 the seawater $B(OH)_4^-/DIC$ ratio we cannot identify whether $B(OH)_4^-$ is the only species incorporated into ACC
 763 based on these data because pH and DIC broadly unavoidably covaried in our experiments. (D) As in panel C,
 764 except further normalised to seawater Ca^{2+} . In panels B and C, the regression only considers data from ACCs
 765 precipitated from seawater with a $[Ca^{2+}]$ close to natural (>4), whereas all data are considered in panel D. Error
 766 estimates propagate the uncertainty in DIC, variation in pH during the titration, and electrode-derived $[Ca^{2+}]$
 767 precision (where relevant).



768

769 **Fig. 8.** Mg incorporation into ACC precipitated from seawater as a function of the solution Mg/Ca ratio. (A)
 770 Compared to calcite resulting from the transformation of ACC in $\text{MgCl}_2\text{-CaCl}_2\text{-NaHCO}_3$ solutions (Blue et al.,
 771 2017) and calcite precipitated from seawater (Mucci and Morse, 1983). H-values refer to the power coefficient of
 772 the least-squares regressions. (B) Compared to ACC precipitated from $\text{MgCl}_2\text{-CaCl}_2\text{-NaHCO}_3/\text{Na}_2\text{CO}_3$ solutions
 773 and at higher solution Mg/Ca ratios (Blue and Dove, 2015).



774
775

776 **Fig. 9.** ACC Mg/Ca ratio as a function of the seawater amino acid concentration. The presence of both aspartic
777 and glutamic acid result in significantly reduced ACC Mg/Ca at amino acid concentrations $> \sim 2$ mM, as
778 expected given the preferential affinity for these amino acids to form ligands with Mg compared to Ca in
779 solution (cf. Wang et al., 2009).
780

781 **Tab. 1.** Seawater chemistry conditions and titration details, resulting precipitate element/Ca ratios, and calculated distribution coefficients. Experiments were conducted from
782 three different seawater reservoirs, made according to the same recipe but with minor differences in their trace element composition (see the supplementary material for full
783 characterisation). Trace element ratios are given in $\mu\text{mol mol}^{-1}$ in the case of Li/Ca, B/Ca, Mn/Ca, and Ba/Ca, mmol mol^{-1} in the case of Na/Ca, Mg/Ca and Sr/Ca, and nmol
784 mol^{-1} in the case of U/Ca. D_B and D_U are calculated using (e.g.) the seawater B/Ca ratio for consistency, but especially in the case of boron are more appropriately described as
785 a function of the seawater carbonate system (see the text and supplementary material for an exploration of this).

| principal variable | pH (NBS) | DIC (μM) | titration rate (ml/min) | seawater [Ca] (mM) | seawater [Mg] (mM) | seawater reservoir | AA conc. (mM) | Li/Ca | B/Ca | Na/Ca | Mg/Ca | Mn/Ca | Sr/Ca | Ba/Ca | U/Ca | D_{Li} ($\times 10^{-3}$) | D_B | D_{Na} ($\times 10^{-3}$) | D_{Mg} | D_{Mn} | D_{Sr} | D_{Ba} | D_U | |
|----------------------------------|----------|-----------------------|-------------------------|--------------------|--------------------|--------------------|---------------|--------|-------|--------|--------|-------|-------|-------|-------|-------------------------------|-------|-------------------------------|----------|----------|----------|----------|-------|------|
| pH/DIC | 9.21 | 17750 | 0.5 | 14.0 | 53.0 | 1 | | 3.14 | 1034 | 64.5 | 363.6 | 127 | 4.47 | 492 | 132 | 1.12 | 0.032 | 1.86 | 0.096 | 27.0 | 0.68 | 2.09 | 0.12 | |
| | 9.58 | 14164 | 0.5 | 12.5 | 53.0 | 1 | | 6.39 | 1275 | 67.0 | 388.5 | 178 | 4.51 | 488 | 150 | 2.02 | 0.035 | 1.72 | 0.091 | 33.8 | 0.61 | 1.84 | 0.12 | |
| | 10.08 | 9953 | 0.5 | 14.3 | 53.0 | 1 | | 3.71 | 2197 | 70.4 | 568.5 | 627 | 4.25 | 451 | 236 | 1.34 | 0.068 | 2.06 | 0.153 | 135.8 | 0.66 | 1.94 | 0.22 | |
| | 8.95 | 24848 | 0.5 | 15.1 | 53.0 | 1 | | 4.10 | 941 | 67.3 | 253.2 | 102 | 4.06 | 514 | 122 | 1.57 | 0.031 | 2.09 | 0.072 | 23.5 | 0.67 | 2.35 | 0.12 | |
| | 9.60 | 14430 | 0.2 | 12.7 | 53.0 | 1 | | 3.14 | 1479 | 60.9 | 370.6 | 186 | 4.57 | 478 | 145 | 1.01 | 0.041 | 1.60 | 0.089 | 36.0 | 0.63 | 1.84 | 0.12 | |
| | 9.60 | 13075 | 1.0 | 13.4 | 53.0 | 1 | | 3.31 | 1480 | 60.4 | 361.4 | 182 | 4.59 | 483 | 147 | 1.12 | 0.043 | 1.66 | 0.091 | 36.9 | 0.66 | 1.95 | 0.13 | |
| | 8.95 | 21639 | 0.5 | 16.0 | 53.0 | 1 | | 4.72 | 1069 | 91.2 | 429.0 | 80 | 5.24 | 364 | 109 | 1.91 | 0.037 | 2.99 | 0.129 | 19.3 | 0.91 | 1.76 | 0.12 | |
| | 9.22 | 18119 | 0.5 | 13.5 | 53.0 | 1 | | 6.24 | 1301 | 125.2 | 433.0 | 124 | 5.22 | 384 | 123 | 2.13 | 0.038 | 3.47 | 0.110 | 25.4 | 0.76 | 1.56 | 0.11 | |
| | 9.52 | 14789 | 0.5 | 13.2 | 53.0 | 1 | | 5.16 | 1374 | 81.2 | 425.3 | 156 | 5.11 | 416 | 125 | 1.72 | 0.039 | 2.20 | 0.105 | 31.1 | 0.73 | 1.65 | 0.11 | |
| | 9.80 | 12414 | 0.5 | 12.8 | 53.0 | 1 | | 3.88 | 1636 | 59.2 | 474.4 | 257 | 5.01 | 418 | 131 | 1.25 | 0.045 | 1.56 | 0.114 | 49.9 | 0.69 | 1.61 | 0.11 | |
| 10.11 | 9739 | 0.5 | 12.1 | 53.0 | 1 | | 2.13 | 1999 | 28.1 | 679.8 | 991 | 4.99 | 374 | 185 | 0.65 | 0.053 | 0.70 | 0.155 | 182.1 | 0.65 | 1.37 | 0.15 | | |
| [Mg] | 9.66 | 9639 | 0.5 | 13.0 | 30.0 | 2 | | 4.52 | 1176 | 58.4 | 315.7 | 165 | 5.94 | 270 | 111 | 1.31 | 0.032 | 1.60 | 0.135 | 27.3 | 0.77 | 0.72 | 0.09 | |
| | 9.64 | 11804 | 0.5 | 13.2 | 40.0 | 2 | | 3.78 | 1388 | 43.5 | 333.0 | 210 | 5.49 | 297 | 127 | 1.11 | 0.038 | 1.19 | 0.109 | 35.2 | 0.72 | 0.81 | 0.10 | |
| | 9.62 | 12489 | 0.5 | 12.9 | 50.0 | 2 | | 3.50 | 1359 | 44.2 | 385.1 | 185 | 5.27 | 316 | 127 | 1.00 | 0.036 | 1.17 | 0.098 | 30.2 | 0.68 | 0.84 | 0.10 | |
| [Ca] | 9.97 | 8177 | 0.5 | 18.8 | 53.0 | 1 | | 5.47 | 1726 | 92.6 | 373.0 | 233 | 3.34 | 544 | 308 | 2.61 | 0.071 | 3.57 | 0.133 | 66.7 | 0.68 | 3.10 | 0.38 | |
| | 10.09 | 4176 | 0.5 | 46.1 | 53.0 | 1 | | 2.11 | 2331 | 44.0 | 254.4 | 416 | 1.53 | 428 | 307 | 2.46 | 0.234 | 4.06 | 0.221 | 291.8 | 0.76 | 5.97 | 0.94 | |
| | 9.54 | 8734 | 0.5 | 21.1 | 53.0 | 2 | | 3.33 | 1400 | 45.0 | 366.3 | 129 | 3.74 | 336 | 130 | 1.57 | 0.061 | 1.94 | 0.146 | 34.6 | 0.79 | 1.46 | 0.17 | |
| | 9.56 | 5809 | 0.5 | 31.2 | 53.0 | 2 | | 9.51 | 1310 | 34.3 | 221.1 | 119 | 2.45 | 358 | 193 | 6.61 | 0.084 | 2.16 | 0.130 | 47.1 | 0.76 | 2.31 | 0.37 | |
| | 9.64 | 4289 | 0.5 | 41.7 | 53.0 | 2 | | 6.15 | 1305 | 31.0 | 173.4 | 135 | 1.92 | 366 | 170 | 5.71 | 0.112 | 2.60 | 0.136 | 71.5 | 0.80 | 3.15 | 0.44 | |
| | 9.65 | 2914 | 0.5 | 51.3 | 53.0 | 2 | | 8.86 | 1144 | 24.1 | 122.3 | 241 | 1.54 | 409 | 215 | 10.13 | 0.121 | 2.46 | 0.118 | 157.4 | 0.79 | 4.34 | 0.68 | |
| [Asp] | 10.05 | 11057 | 0.5 | 12.4 | 53.0 | 1 | 2.5 | 4.12 | 1906 | 87.7 | 504.2 | 447 | 4.29 | 467 | 216 | 1.29 | 0.051 | 2.23 | 0.118 | 83.9 | 0.57 | 1.74 | 0.18 | |
| | 9.64 | - | 0.5 | - | 53.0 | 1 | 2.6 | 3.25 | 1449 | 41.4 | 360.4 | 140 | 5.02 | 487 | 135 | - | - | - | - | - | - | - | - | |
| | 9.59 | 12474 | 0.5 | 12.8 | 53.0 | 2 | 5.4 | 3.59 | 1357 | 50.1 | 345.2 | 137 | 5.08 | 336 | 142 | 1.03 | 0.036 | 1.32 | 0.084 | 22.3 | 0.65 | 0.89 | 0.11 | |
| Asp+Glu | 9.53 | 13364 | 0.5 | 11.7 | 53.0 | 1 | 10.2 | 3.52 | 1225 | 46.9 | 267.5 | 91 | 4.88 | 473 | 133 | 1.05 | 0.031 | 1.13 | 0.059 | 16.3 | 0.62 | 1.68 | 0.10 | |
| | 9.56 | 15264 | 0.5 | 15.6 | 53.0 | 1 | 20.0 | - | 1454 | 62.1 | 266.3 | 75 | 4.09 | 476 | 141 | - | 0.049 | 1.98 | 0.078 | 17.7 | 0.69 | 2.24 | 0.15 | |
| | 9.55 | 16375 | 0.5 | 16.7 | 53.0 | 1 | 40.0 | 4.58 | 1281 | 69.4 | 227.5 | 55 | 4.01 | 492 | 112 | 1.93 | 0.046 | 2.37 | 0.072 | 14.0 | 0.72 | 2.48 | 0.12 | |
| | [Glu] | 10.05 | 11138 | 0.5 | 12.4 | 53.0 | 1 | 2.0 | 2.87 | 1766 | 69.2 | 582.9 | 483 | 4.43 | 427 | 205 | 0.91 | 0.048 | 1.77 | 0.137 | 91.3 | 0.60 | 1.60 | 0.17 |
| | 9.63 | 12744 | 0.5 | 13.1 | 53.0 | 2 | 2.5 | 2.77 | 1464 | 40.1 | 351.6 | 188 | 4.98 | 342 | 146 | 0.81 | 0.040 | 1.08 | 0.087 | 31.4 | 0.65 | 0.93 | 0.12 | |
| | 9.60 | 13519 | 0.5 | 12.9 | 53.0 | 2 | 4.7 | 2.89 | 1420 | 41.5 | 343.9 | 168 | 5.02 | 338 | 141 | 0.83 | 0.038 | 1.10 | 0.084 | 27.5 | 0.65 | 0.90 | 0.11 | |
| calcites or calcite/ACC mixtures | 9.57 | 14324 | 0.5 | 12.7 | 53.0 | 2 | 9.9 | 3.42 | 1342 | 45.0 | 282.2 | 143 | 4.78 | 353 | 135 | 0.97 | 0.035 | 1.18 | 0.068 | 23.2 | 0.61 | 0.93 | 0.11 | |
| | 9.61 | 15933 | 0.5 | 16.2 | 53.0 | 1 | 20.0 | 3.22 | 1361 | 69.1 | 281.1 | 110 | 3.97 | 468 | 139 | 1.32 | 0.048 | 2.30 | 0.086 | 27.0 | 0.70 | 2.29 | 0.15 | |
| | 9.58 | - | 0.5 | 10.3 | 0.1 | 3 | | 19.79 | 2474 | 28.2 | 0.1 | 7 | 1.65 | 422 | 231 | 5.16 | 0.055 | 0.60 | 0.014 | 1.0 | 0.18 | 1.31 | 0.16 | |
| | 10.01 | 4504 | 0.5 | - | 5.0 | 3 | | 49.50 | 536 | 40.1 | 21.2 | 12 | 4.68 | 322 | 1 | - | - | - | - | - | - | - | - | |
| | 9.76 | 11088 | 0.5 | 13.5 | 10.0 | 3 | | 18.20 | 850 | 69.8 | 65.6 | 56 | 5.56 | 560 | 0 | 6.22 | 0.025 | 2.03 | 0.088 | 38.6 | 1.02 | 1.84 | 0.01 | |
| | 9.85 | 5350 | 0.5 | - | 10.0 | 3 | | 43.44 | 653 | 38.2 | 21.6 | 18 | 3.48 | 371 | 2 | - | - | - | - | - | - | - | - | |
| | 9.58 | 6820 | 0.5 | 13.1 | 10.0 | 3 | | 5.17 | 772 | 65.3 | 38.2 | 6 | 4.79 | 554 | 2 | 1.72 | 0.022 | 1.85 | 0.050 | 4.0 | 0.85 | 1.77 | 0.04 | |
| | 9.72 | - | 0.5 | - | 10.0 | 3 | | 44.94 | 569 | 39.4 | 33.8 | 28 | 3.88 | 342 | 1 | - | - | - | - | - | - | - | - | |
| | 9.60 | 6289 | 0.5 | 11.7 | 10.3 | 3 | | 44.51 | 633 | 33.7 | 29.6 | 35 | 3.98 | 144 | 247 | 11.56 | 0.015 | 0.85 | 0.033 | 5.2 | 0.46 | 0.35 | 0.18 | |
| | 9.61 | 7994 | 0.5 | 12.4 | 20.3 | 3 | | 52.64 | 407 | 25.1 | 76.1 | 69 | 4.15 | 212 | 488 | 14.50 | 0.010 | 0.66 | 0.046 | 10.8 | 0.51 | 0.54 | 0.37 | |
| brucites | 10.36 | 8971 | 0.5 | 13.3 | 53.0 | 1 | | 118.23 | 22770 | 1749.4 | 6339.6 | 781 | 3.81 | 441 | 6968 | 39.72 | 0.657 | 47.75 | 1.587 | 157.5 | 0.55 | 1.77 | 6.13 | |
| | 10.21 | - | 0.5 | - | 53.0 | 1 | | 17.22 | 26983 | 293.0 | 7823.4 | 1415 | 3.62 | 340 | 10130 | - | - | - | - | - | - | - | - | |

787 **References**

788

- 789 Allison N., Cohen I., Finch A. a, Erez J. and Tudhope A. W. (2014) Corals concentrate dissolved
790 inorganic carbon to facilitate calcification. *Nat. Commun.* **5**, 5741.
- 791 Andersen F. A. and Brečević L. (1991) Infrared spectra of amorphous and crystalline calcium
792 carbonate. *Acta Chem. Scand.* **45**, 1018–1024.
- 793 Beniash E., Aizenberg J., Addadi L., Weiner S. and B P. R. S. L. (1997) Amorphous calcium carbonate
794 transforms into calcite during sea urchin larval spicule growth Amorphous calcium carbonate
795 transforms into calcite during sea urchin larval spicule growth. *Proc. R. Soc. London B* **264**, 461–
796 465.
- 797 Bentov S., Brownlee C. and Erez J. (2009) The role of seawater endocytosis in the biomineralization
798 process in calcareous foraminifera. *Proc. Natl. Acad. Sci. U. S. A.* **106**, 21500–4.
- 799 Bentov S. and Erez J. (2006) Impact of biomineralization processes on the Mg content of foraminiferal
800 shells: A biological perspective. *Geochemistry Geophys. Geosystems* **7**.
- 801 Blue C. R. and Dove P. M. (2015) Chemical controls on the magnesium content of amorphous
802 calcium carbonate. *Geochim. Cosmochim. Acta* **148**, 23–33.
- 803 Blue C. R., Giuffre A., Mergelsberg S., Han N., Yoreo J. J. De and Dove P. M. (2017) Chemical and
804 physical controls on the transformation of amorphous calcium carbonate into crystalline CaCO
805 3 polymorphs. **196**, 179–196.
- 806 Branson O. (2018) Boron Incorporation into Marine CaCO₃. In *Boron Isotopes. Advances in Isotope*
807 *Geochemistry.* (eds. H. Marshall and G. Foster). Springer, Cham.
- 808 Brecevic L. and Nielsen A. E. (1989) Solubility of amorphous calcium carbonate. **98**, 504–510.
- 809 Burton E. A. and Walter L. M. (1991) The effects of P_cO₂ and temperature on ~ nesium incorpo ~ tion
810 in calcite in seawater and MgC₁₂-CaC₁₂ solutions. **55**, 777–785.
- 811 Busenberg E. and Plummer L. N. (1986) The solubility of BaCO₃(cr) (witherite) in CO₂-H₂O
812 solutions between 0 and 90oC, evaluation of the association constants of BaHCO₃ (aq) and
813 BaCO₃ (aq) between 5 and 80oC , and a preliminary evaluation of the thermodynamic
814 properties of Ba²⁺ (aq). *Geochim. Cosmochim. Acta* **50**, 2225–2233.
- 815 Busenberg E. and Plummer L. N. (1984) The solubility of strontianite (SrCO₃) in CO₂-H₂O solutions
816 between 2 and 91oC, the association constants of STHCO₃+(aq) and SrCO₃(aq) between 5 and
817 80oC, and an evaluation of the thermodynamic properties of Sr²⁺(aq) and SrCO₃ (cr) at 25oC
818 and 1 atm tota. *Geochim. Cosmochim. Acta* **48**.
- 819 De Choudens-Sanchez V. and Gonzalez L. a. (2009) Calcite and Aragonite Precipitation Under
820 Controlled Instantaneous Supersaturation: Elucidating the Role of CaCO₃ Saturation State and
821 Mg/Ca Ratio on Calcium Carbonate Polymorphism. *J. Sediment. Res.* **79**, 363–376.
- 822 Decarlo T. M., Gaetani G. A., Holcomb M. and Cohen A. L. (2015) Experimental determination of
823 factors controlling U/Ca of aragonite precipitated from seawater : Implications for interpreting
824 coral skeleton. *Geochim. Cosmochim. Acta* **162**, 151–165.
- 825 Decarlo T. M., Holcomb M. and McCulloch M. T. (2018) Reviews and syntheses: Revisiting the boron
826 systematics of aragonite and their application to coral calcification. *Biogeosciences* **15**, 2819–
827 2834.
- 828 DePaolo D. J. (2011) Surface kinetic model for isotopic and trace element fractionation during
829 precipitation of calcite from aqueous solutions. *Geochim. Cosmochim. Acta* **75**, 1039–1056.
- 830 Dickson A. G. (1990) Thermodynamics of the dissociation of boric acid in synthetic seawater from
831 273.15 to 318.15 K. *Deep Sea Res.* **37**, 755–766.
- 832 Dickson A. G. and Millero F. J. (1987) A comparison of the equilibrium constants for the dissociation

833 of carbonic acid in seawater media. *Deep Sea Res.* **34**, 1733–1743.

834 Dietzel M., Gussone N. and Eisenhauer A. (2004) Co-precipitation of Sr²⁺ and Ba²⁺ with aragonite
835 by membrane diffusion of CO₂ between 10 and 50 °C. *Chem. Geol.* **203**, 139–151.

836 Erez J. (2003) The source of ions for biomineralization in foraminifera and their implications for
837 paleoceanographic proxies (Review). *Rev. Mineral. geochemistry* **54**, 115.

838 Evans D., Erez J., Oron S. and Müller W. (2015) Mg/Ca-temperature and seawater-test chemistry
839 relationships in the shallow-dwelling large benthic foraminifera *Operculina ammonoides*.
840 *Geochim. Cosmochim. Acta* **148**, 325–342.

841 Evans D., Müller W. and Erez J. (2018) Assessing foraminifera biomineralisation models through
842 trace element data of cultures under variable seawater chemistry. *Geochim. Cosmochim. Acta*.

843 Evans D., Webb P., Penkman K. E. H., Kroger R. and Allison N. (2019) The characteristics and
844 biological relevance of inorganic amorphous calcium carbonate (ACC) precipitated from
845 seawater. *Cryst. Growth Des.*

846 Föger A., Konrad F., Leis A., Dietzel M. and Mavromatis V. (2019) Effect of growth rate and pH on
847 lithium incorporation in calcite. *Geochim. Cosmochim. Acta* **248**, 14–24.

848 Gagnon A. C., Adkins J. F. and Erez J. (2012) Seawater transport during coral biomineralization. *Earth*
849 *Planet. Sci. Lett.* **329–330**, 150–161.

850 Giuffrè A. J., Gagnon A. C., De Yoreo J. J. and Dove P. M. (2015) Isotopic tracer evidence for the
851 amorphous calcium carbonate to calcite transformation by dissolution-reprecipitation. *Geochim.*
852 *Cosmochim. Acta* **165**, 407–417.

853 Hain M. P., Sigman D. M., Higgins J. A. and Haug G. H. (2015) The effects of secular calcium and
854 magnesium concentration changes on the thermodynamics of seawater acid/base chemistry:
855 Implications for Eocene and Cretaceous ocean carbon chemistry and buffering. *Glob.*
856 *Biogeochem. Cycles* **29**, 517–533.

857 Hauzer H., Evans D., Müller W., Rosenthal Y. and Erez J. (2018) Calibration of Na partitioning in the
858 calcitic foraminifer *Operculina ammonoides* under variable Ca concentration: Toward
859 reconstructing past seawater composition. *Earth Planet. Sci. Lett.* **497**, 80–91.

860 Holcomb M., DeCarlo T. M., Gaetani G. A. and McCulloch M. (2016) Factors affecting B/Ca ratios in
861 synthetic aragonite. *Chem. Geol.* **437**, 67–76.

862 Ishikawa M. and Ichikuni M. (1984) Uptake of sodium and potassium by calcite. *Chem. Geol.* **42**, 137–
863 146.

864 Jacob D. E., Wirth R., Agbaje O. B. A., Branson O. and Eggins S. M. (2017) Planktic foraminifera form
865 their shells via metastable carbonate phases. *Nat. Commun.* **8**, 1–8.

866 Johnson K. S. (1982) Solubility of rhodochrosite (MnCO₃) in water and seawater. *Geochim.*
867 *Cosmochim. Acta* **46**, 1805–1809.

868 Keul N., Langer G., De Nooijer L. J., Nehrke G., Reichart G. J. and Bijma J. (2013) Incorporation of
869 uranium in benthic foraminiferal calcite reflects seawater carbonate ion concentration.
870 *Geochemistry, Geophys. Geosystems* **14**, 102–111.

871 Kim Y.-Y., Carloni J. D., Demarchi B., Sparks D., Reid D. G., Kunitake M. E., Tang C. C., Duer M. J.,
872 Freeman C. L., Pokroy B., Penkman K., Harding J. H., Estroff L. A., Baker S. P. and Meldrum F.
873 C. (2016) Tuning hardness in calcite by incorporation of amino acids. *Nat. Mater.* **in press**, DOI:
874 10.1038/nmat4631.

875 King J. K. and Hare P. E. (1972) Amino acid composition of the test as a taxonomic character for
876 living and fossil planktonic foraminifera. *Micropaleontology* **18**, 285–293.

877 Kitano Y., Kanamori N. and Oomori T. (1971) Measurement of distribution coefficients of strontium
878 and barium between carbonate precipitate and solution - Abnormally high values of distribution

879 coefficients measured at early stages of carbonate formation. *Geochem. J.* **4**, 183–206.

880 Konrad F., Gallien F., Gerard D. E. and Dietzel M. (2016) Transformation of Amorphous Calcium
881 Carbonate in Air. *Cryst. Growth Des.* **16**, 6310–6317.

882 Lam R. S. K., Charnock J. M., Lennie A. and Meldrum F. C. (2007) Synthesis-dependant structural
883 variations in amorphous calcium carbonate. *CrystEngComm* **9**, 1226–1236.

884 Lewis E. and Wallace D. (1998) *Program developed for CO₂ system calculations.*, Upton, New York.

885 Marriott C. S., Henderson G. M., Belshaw N. S. and Tudhope A. W. (2004) Temperature dependence
886 of $\delta^{7}\text{Li}$, $\delta^{44}\text{Ca}$ and Li/Ca during growth of calcium carbonate. *Earth Planet. Sci. Lett.* **222**, 615–
887 624.

888 Mavromatis V., Goetschl K. E., Grengg C., Konrad F., Purgstaller B. and Dietzel M. (2018)
889 ScienceDirect Barium partitioning in calcite and aragonite as a function of growth rate. **237**, 65–
890 78.

891 McCulloch M. T., D’Olivo J. P., Falter J., Holcomb M. and Trotter J. A. (2017) Coral calcification in a
892 changing World and the interactive dynamics of pH and DIC upregulation. *Nat. Commun.* **8**, 1–
893 8.

894 Millero F. J. (2013) *Chemical Oceanography*. 4th ed., Taylor & Francis Group, Boca Raton.

895 Mucci A. (1988) Manganese uptake during calcite precipitation from seawater: Conditions leading to
896 the formation of a pseudokutnahorite. *Geochim. Cosmochim. Acta* **52**, 1859–1868.

897 Mucci A. and Morse J. W. (1983) The incorporation of Mg^{2+} and Sr^{2+} into calcite overgrowths:
898 influences of growth rate and solution composition. *Geochim. Cosmochim. Acta* **47**, 217–233.

899 Nehrke G., Reichart G. J., Van Cappellen P., Meile C. and Bijma J. (2007) Dependence of calcite
900 growth rate and Sr partitioning on solution stoichiometry: Non-Kossel crystal growth. *Geochim.*
901 *Cosmochim. Acta* **71**, 2240–2249.

902 de Nooijer L. J., Spero H. J., Erez J., Bijma J. and Reichart G. J. (2014) Biomineralization in perforate
903 foraminifera. *Earth-Science Rev.* **135**, 48–58.

904 de Nooijer L. J., Toyofuku T. and Kitazato H. (2009) Foraminifera promote calcification by elevating
905 their intracellular pH. *Proc. Natl. Acad. Sci. U. S. A.* **106**, 15374–15378.

906 Okumura M. and Kitano Y. (1986) Coprecipitation of alkali metal ions with calcium carbonate.
907 *Geochim. Cosmochim. Acta* **50**, 49–58.

908 Parkhurst D. L. and Appelo C. A. J. (1999) *User’s Guide to PHREEQC — a Computer Program for*
909 *Speciation, Batch-Reaction, One-dimensional Transport, and Inverse Geochemical Calculations.*,

910 Politi B. Y., Levi-kalishman Y., Raz S., Wilt F., Addadi L., Weiner S. and Sagi I. (2006) Structural
911 Characterization of the Transient Amorphous Calcium Carbonate Precursor Phase in Sea
912 Urchin Embryos **, 1289–1298.

913 Purgstaller B., Goetschl K. E., Mavromatis V. and Dietzel M. (2019) Solubility investigations in the
914 amorphous calcium magnesium carbonate system. *CrystEngComm* **21**, 155–164.

915 Reeder R. J., Elzinga E. J., Tait C. D., Rector K. D., Donohoe R. J. and Morris D. E. (2004) Site-specific
916 incorporation of uranyl carbonate species at the calcite surface. *Geochim. Cosmochim. Acta* **68**,
917 4799–4808.

918 Reeder R. J., Nugent M., Lambie G. M., Tait C. D. and Morris D. E. (2000) Uranyl incorporation into
919 calcite and aragonite: XAFS and luminescence studies. *Environ. Sci. Technol.* **34**, 638–644.

920 Sviben S., Gal A., Hood M. A., Bertinetti L., Politi Y., Bennet M., Krishnamoorthy P., Schertel A.,
921 Wirth R., Sorrentino A., Pereiro E., Faivre D. and Scheffel A. (2016) A vacuole-like compartment
922 concentrates a disordered calcium phase in a key coccolithophorid alga. *Nat. Commun.* **7**, 11228.

923 Uchikawa J., Penman D. E., Zachos J. C. and Zeebe R. E. (2015) Experimental evidence for kinetic
924 effects on B/Ca in synthetic calcite: Implications for potential $\text{B}(\text{OH})_4^-$ and $\text{B}(\text{OH})_3$

925 incorporation. *Geochim. Cosmochim. Acta* **150**, 171–191.

926 Wang D., Wallace A. F., De Yoreo J. J. and Dove P. M. (2009) Carboxylated molecules regulate
927 magnesium content of amorphous calcium carbonates during calcification. *Proc. Natl. Acad. Sci.*
928 *U. S. A.* **106**, 21511–6.

929 Watson E. B. (2004) A conceptual model for near-surface kinetic controls on the trace- element and
930 stable isotope composition of abiogenic calcite crystals. *Geochim. Cosmochim. Acta* **68**, 1473–
931 1488.

932 Weremeichik J. M., Gabitov R. I., Thien B. M. J. and Sadekov A. (2017) The effect of growth rate on
933 uranium partitioning between individual calcite crystals and fluid. *Chem. Geol.* **450**, 145–153.

934 White A. F. (1977) Sodium and potassium coprecipitation in aragonite. *Geochim. Cosmochim. Acta*
935 **41**, 613–625.

936 White A. F. (1978) Sodium coprecipitation in calcite and dolomite. *Chem. Geol.* **23**, 65–72.

937 Wolthers M., Nehrke G., Gustafsson J. P. and Van Cappellen P. (2012) Calcite growth kinetics:
938 Modeling the effect of solution stoichiometry. *Geochim. Cosmochim. Acta* **77**, 121–134.

939